Assessment of source contributions to seasonal vegetative exposure to ozone in the U.S.

Kateryna Lapina,[1] Daven K. Henze,[1] Jana B. Milford,[1] Min Huang,[2,3] Meiyun Lin,[4,5] Arlene M. Fiore,[6] Greg Carmichael,[3] Gabriele G. Pfister[7] and Kevin Bowman[2]

Corresponding author: K. Lapina, ECME 114, 1111 Engineering Dr, University of Colorado, Boulder, CO 80309, USA (kateryna.lapina@colorado.edu)

[1]Department of Mechanical Engineering, University of Colorado, Boulder, CO, USA

[2]Jet Propulsion Laboratory, California Institute of Technology, Pasadena, CA, USA

[3]Center for Global and Regional Environmental Research, the University of Iowa, Iowa City, IA, USA

[4]Atmospheric and Oceanic Sciences, Princeton University, Princeton, NJ, USA

[5]Geophysical Fluid Dynamics Laboratory, NOAA, Princeton, NJ, USA

This article has been accepted for publication and undergone full peer review but has not been through the copyediting, typesetting, pagination and proofreading process, which may lead to differences between this version and the Version of Record. Please cite this article as doi: 10.1002/2013JD020905

Abstract.

W126 is a cumulative ozone exposure index based on sigmoidally weighted daytime ozone concentrations used to evaluate the impacts of ozone on vegetation. We quantify W126 in the U.S. in the absence of North American anthropogenic emissions (North American background or "NAB") using three regional or global chemical transport models for May–July 2010. All models overestimate W126 in the eastern U.S. due to a persistent bias in daytime ozone, while the models are relatively unbiased in California and the intermountain West. Substantial difference in the magnitude and spatial and temporal variability of the estimates of W126 NAB between models supports the need for a multi-model approach. While the average NAB contribution to daytime ozone in the intermountain West is 64–78%, the average W126 NAB is only 9–27% of current levels, owing to the weight given to high O_3 concentrations in W126. Based on a three-model mean, NAB explains ∼30%

[6]Department of Earth and Environmental
Sciences and Lamont-Doherty Earth
Observatory, Columbia University,
Palisades, NY, USA

[7]Atmospheric Chemistry Division,
National Center for Atmospheric Research
(NCAR), Boulder, CO, USA

of the daily variability in the W126 daily index in the intermountain West. Adjoint sensitivity analysis shows that nationwide W126 is influenced most by NO_x emissions from anthropogenic (58% of the total sensitivity) and natural (25%) sources followed by non-methane volatile organic compounds (10%) and CO (7%). Most of the influence of anthropogenic NO_x comes from the U.S. (80%), followed by Canada (9%), Mexico (4%) and China (3%). Thus, long-range transport of pollution has a relatively small impact on W126 in the U.S., and domestic emissions control should be effective for reducing W126 levels.

1. Introduction

Accumulated exposure to elevated levels of ozone leads to detrimental effects on vegetation [*e.g.*, *Reich and Amundson*, 1985; *Chappelka et al.*, 1999; *Schaub et al.*, 2005]. Thus, present-day ozone levels are shown to cause significant yield reduction for a number of major crops on a global scale, leading to substantial economic losses annually [*e.g.*, *Van Dingenen et al.*, 2009; *Avnery et al.*, 2011]. Studies have also documented numerous other negative impacts on ecosystems, such as reductions in tree growth, decreases in photosynthetic rates and visible foliar injuries on multiple plant species, including deciduous trees in eastern North America and coniferous trees in the western U.S. [*e.g.*, *U.S. EPA*, 2006; *Arbaugh et al.*, 1998; *Schaub et al.*, 2005]. Recent research has focused on reduction of ozone levels through mitigation of conventional short-lived ozone precursors (e.g., NO_x, non-methane volatile organic compounds (NMVOCs) and CO), as well as reduction in methane [*Shindell et al.*, 2012; *Avnery et al.*, 2013] and even cultivation of ozone-resistant crops to minimize crop production losses [*Avnery et al.*, 2013]. In North America (NA) the economic loss due to ozone damage for four ozone-sensitive crops (wheat, rice, soybean and maize) is estimated to be between 3 to 5.5 billion US dollars in 2000 [*Van Dingenen et al.*, 2009], depending on the ozone metric used. *Hollaway et al.* [2012] have further demonstrated that while most of the crop yield loss can be mitigated through local emissions controls, trans-boundary impacts are not negligible, with SE Asian emissions responsible for 2.3% of crop yield loss for soybeans in North America in 2000.

The Clean Air Act requires the U.S. EPA to set two National Ambient Air Quality Standards for criteria pollutants such as ground-level ozone — a primary standard, which

serves to protect human health, and a secondary standard with a purpose to protect ecosystems and crops. A number of metrics can be used to evaluate vegetative exposure to ozone, including seasonal 7 h and 12 h mean daytime ozone concentrations (M7 and M12 respectively), and seasonal cumulative exposure above 40 and 60 ppbv (AOT40, which is the current standard in Europe, and SUM60, respectively). Cumulative metrics emphasizing high concentrations are considered to be better suited for relating vegetative response to ambient ozone exposure [*U.S. EPA*, 2013]. The metric considered for the secondary standard in the U.S. is W126, a biologically based index that estimates a cumulative ozone exposure over a 3-month growing season and applies sigmoidal weighting to hourly ozone concentrations [*Lefohn and Runeckles*, 1987; *Lefohn et al.*, 1988]. An advantage of W126 over other cumulative metrics is that it does not employ a threshold but applies weights which increase with higher concentrations, potentially more detrimental for vegetation [*U.S. EPA*, 2013]. Several U.S. counties are projected to violate a potential W126 standard of 13 ppm-hrs, even if they are not in violation of a primary standard set at 70 ppbv [*U.S. EPA*, 2011]. Many of the counties with high W126 are located in rural areas, mostly in the West, that lack significant local emissions, and vegetative damage at these sites results from ozone or ozone precursors transported from other regions.

From a regulatory standpoint, the U.S. EPA distinguishes between ozone formed from sources that could be controlled through emission regulations in North America and ozone that is not affected by such emissions —the North American Background (NAB). The NAB includes contributions from natural sources and long-range transport of ozone and its precursors from outside North America. Previous estimates of NAB found higher values in the mountainous western U.S. compared to the East [*Fiore et al.*, 2003; *Wang*

et al., 2009; *Emery et al.*, 2012; *Lin et al.*, 2012a] with the maximum daily average 8-hour ozone (MDA8) NAB concentrations reaching 50–60 ppbv in spring and summer in the intermountain West [*Zhang et al.*, 2011; *Emery et al.*, 2012], and occasionally being as high as 75 ppbv during stratospheric intrusion events [*Lin et al.*, 2012b]. NAB ozone was found to be correlated with total ozone in the West, contributing substantially to high-ozone days, while no such correlation was found in the East [*Fiore et al.*, 2003; *Zhang et al.*, 2011]. Because of the different nature of the metrics used for primary and potential secondary ozone standards and the fact that the attainment of the primary standard will not necessarily ensure the attainment of the W126-based standard, especially in rural regions, there is a need to estimate how NAB levels contribute specifically to W126.

The North American Background can only be estimated by chemical transport models (CTMs). CTMs have been widely used for source sensitivity analysis of ozone pollution, with several general approaches being applied, including brute-force calculations, tracer tagging and adjoint simulations. In the first approach, a perturbation is applied to emission sources; comparison to an unperturbed run is then used to infer their influence on model outputs [*e.g.*, *Jacob et al.*, 1999; *Fiore et al.*, 2009]. The tagged tracer approach "tags" emitted pollutants according to their sources, e.g., stratospheric or Asian ozone tracers [*Brown-Steiner and Hess*, 2011]. The adjoint approach considers an infinitesimal variation of a scalar model output, e.g., mean ozone concentration in the U.S., and uses auxiliary equations to propagate sensitivities backward in time during a single adjoint model run to calculate the impact of multiple emission sources and model parameters [*e.g.*, *Sandu et al.*, 2005; *Hakami et al.*, 2006]. The advantage of the adjoint approach

is obtaining spatially resolved sensitivity information for individual emitted species for relatively low computational cost when a scalar model output is considered.

Previous studies on W126 have found it to be a challenging ozone exposure metric to model due to the cumulative nature of the index and sensitivity to model errors for the elevated ozone concentrations where higher weights are applied [*Tong et al.*, 2009; *Hollaway et al.*, 2012]. Comparisons between the mean daily maximum 8-hour average and W126 index also showed that W126 produces a stronger and more nonlinear response to perturbations in transported background ozone [*Huang et al.*, 2013]. Because of this nonlinear nature and high sensitivity to model errors and perturbations, a multi-model approach is valuable for reducing model bias and for estimating uncertainty in W126 source attribution. Additionally, a multi-model approach is strongly recommended for NAB ozone estimation [*McDonald-Buller et al.*, 2011]. In this work we estimate W126 in the absence of NA anthropogenic emissions for May–July 2010 using three chemical transport models: GEOS-Chem, AM3 and STEM. We also quantify spatially and species-resolved relative influences of multiple anthropogenic and natural emission sources on the nationwide W126 metric through application of the GEOS-Chem adjoint model.

2. Methods

2.1. W126 and selection of study period

The W126 ozone index is calculated by applying a sigmoidally-shaped weighting to daytime (8:00–19:59 local time) hourly ozone concentrations and summing them to compute a W126 daily index (DI):

$$DI = \sum_{k=08:00}^{19:59} \frac{[O_3]_k}{1 + 4403e^{(-0.126[O_3]_k)}} \quad (1)$$

where $[O_3]_k$ is hourly ozone concentration in ppbv. This weighting emphasizes high ozone concentrations while retaining mid- and low ozone values. For example, the weights are 0.03 at 40 ppbv and reach 0.6 at an inflection point of 70 ppbv (Figure 1). Ozone values of ∼100 ppbv and above are weighted by 1. Monthly W126 is determined by summing the daily index over all days in a given month, and annual W126 is the maximum sum during a consecutive 3-month period.

The proposed air quality standard selects the 3-month period to obtain an annual W126 for a given location in each year, and the W126 design value is a 3-year mean of these annual values. (Further details on calculating the W126 index can be found on EPA website, http://www.epa.gov/ttn/analysis/w126.htm.) The season with the highest observed ozone concentrations depends on location [*Fiore et al.*, 2003]. For example, the 3-month period with the maximum W126 value varies from April–May–June in Florida to July–August–September in parts of California. This makes modeling the maximum 3-month sum in the continental U.S. computationally expensive. Thus, in this work we focus on a fixed 3-month period, May–July 2010, which encompasses the maximum W126 3-month sum in many regions of the U.S. and corresponds to the mean value of the W126 season in the continental U.S.

2.2. Observations

Hourly ozone observations used in this work are taken from the Air Quality System (AQS) and Clean Air Status and Trends Network (CASTNET). AQS

(http://www.epa.gov/ttn/airs/airsaqs) contains ambient air pollution and meteorological data collected from thousands of monitoring stations across the U.S. CASTNET (http://www.epa.gov/castnet) monitors air quality in rural areas. The data in both networks are subject to strict quality control and quality assurance procedures. To compare models with observations we exclude stations with less than 75% of complete days (thus omitting less than 2% of stations). For the remaining stations, monthly W126 is adjusted for missing observations by applying the ratio of the total number of hours in that month to the number of hours with valid observations. Figure 2a shows the sites used in this work. Data from 1145 AQS and 66 CASTNET monitoring sites are analyzed here.

2.3. Models

Simulations from two global (GEOS-Chem and AM3) and one regional (STEM) chemical transport models are used to estimate the NAB for daytime ozone and W126. We perform two sets of simulations for each model—the "base" scenario, which includes all emissions, and a sensitivity simulation with North American anthropogenic emissions set to zero—the "NAB" scenario. GEOS-Chem adjoint simulations and a tagged stratospheric ozone tracer from AM3 are also used for further source attribution (see Table 1). Surface hourly ozone output from each model is used to compute the W126 index for May–July 2010, as described above (Section 2.1) for the base and NAB cases. Model outputs from the base simulations (with all emissions included) are evaluated using observations from the CASTNET and AQS datasets. The ozone concentrations discussed in the rest of this work will refer to daytime (8:00–19:59 local time) surface ozone values, for consistency with the W126 index. Descriptions of the models used in this work are given below and in Table 2, with further details available from references listed therein.

2.3.1. GEOS-Chem

We use the GEOS-Chem model (www.geos-chem.org) driven by GEOS-5 assimilated meteorology from the NASA Global Modeling Assimilation Office. We use global simulations with $2^\circ \times 2.5^\circ$ horizontal resolution as well as nested NA simulations with horizontal resolution of $1/2^\circ \times 2/3^\circ$, each with 47 vertical levels. Ozone concentrations are output from the midpoint of the first model layer, which is ∼120 m thick. GEOS-Chem includes detailed tropospheric chemistry with anthropogenic emissions from the 2005 National Emission Inventory (NEI2005) for the U.S. scaled to 2006, the Big Bend Regional Aerosol and Visibility Observational study [*Kuhns et al.*, 2005] for Mexico, and from the Criteria Air Contaminants emission estimates for Canada. We use Asian anthropogenic emission estimates prepared for the NASA INTEX-B mission in 2006 [*Zhang et al.*, 2009b], and European emission estimates from the European Monitoring and Evaluation Programme inventory. Biogenic emissions are from the Model of Emissions of Gases and Aerosols from Nature (MEGAN) version 2.0 [*Guenther et al.*, 2006] and biomass burning emissions are taken from the Global Fire Emissions Database version 3 (GFED3) inventory [*van der Werf et al.*, 2010], which includes emissions from both wildfires and fires caused by human activity. The lightning source of NO_x is calculated as a function of GEOS-5 deep convective cloud top heights and scaled to match OTD/LIS climatological observations [*Murray et al.*, 2012]. NO_x emissions from soil are derived from the scheme by *Wang et al.* [1998]. We apply a linearized stratospheric chemistry mechanism as described by *Murray et al.* [2012] and a linearized stratospheric ozone (Linoz) parameterization [*McLinden et al.*, 2000]. *Wu et al.* [2007] have shown that ozone production in GEOS-Chem can be significantly affected by the updates in the yield of organic nitrates from isoprene oxidation.

While a more recent update included a 10% isoprene nitrate yield, the GEOS-Chem version used in this work employs 18%. In the discussion below we consider the implications of using this value on the model results.

2.3.2. STEM

The Sulfur Transport and dEposition Model (STEM) has been used and evaluated in a number of field campaigns [*Carmichael et al.*, 2003; *Adhikary et al.*, 2010; *Huang et al.*, 2010]. The full-chemistry version of STEM (2K3) used here calculates gas-phase chemistry reactions based on the SAPRC 99 chemical mechanism [*Carter*, 2000] with thirty photolysis rates calculated online by the Tropospheric UltraViolet Radiation model. The STEM base and NAB simulations are performed over North America on a 60×60 km Lambert Conformal conic projection grid with 18 vertical layers from surface to top of the troposphere (∼11–12 km), with a ∼60-m thick surface layer. Meteorological fields are generated by the Advanced Research Weather Research and Forecasting Model (WRF-ARW) version 3.3.1 driven by National Centers for Environmental Prediction final analysis on $1^\circ \times 1^\circ$ grid every six hours data (http://www.mmm.ucar.edu/wrf/OnLineTutorial/DATA/FNL/index.html). The physics options used for the WRF simulation are similar to *Huang et al.* [2013]. Anthropogenic emissions are taken from NEI2005. Biomass burning emissions are from the FINN inventory v1.0 (http://bai.acd.ucar.edu/Data/fire/; *Wiedinmyer et al.* [2011]) and are placed into multiple model layers. Biogenic emissions are generated by MEGAN version 2.1 based on the WRF meteorology (http://acd.ucar.edu/∼guenther/MEGAN/MEGAN.htm; *Guenther et al.* [2012]). Lightning NO_x emissions are generated following the method described by *Allen et al.* [2012], with the flash rates determined by the WRF convective

precipitation and scaled to the National Lightning Detection Network flash rates. The emissions are vertically distributed to multiple model layers, based on *Ott et al.* [2010]. STEM uses the time-varying lateral and top boundary conditions downscaled from the base and NAB 2° × 2.5° GEOS-Chem simulations (saved hourly).

2.3.3. AM3

The Geophysical Fluid Dynamics Laboratory AM3 global chemistry-climate model (GFDL AM3) nudged to reanalysis winds has been recently applied to quantify Asian and stratospheric influences on springtime high surface ozone events in the western U.S. [*Lin et al.*, 2012b, a]. The model includes fully coupled stratospheric and tropospheric chemistry, described in more detail by *Lin et al.* [2012b] and *Naik et al.* [2013]. Analysis of daily ozonesonde and surface measurements during the CalNex field campaign in May–June 2010 (http://www.esrl.noaa.gov/csd/projects/calnex/) indicates that AM3 captures key features of ozone day-to-day variability in the free troposphere and at surface sites over the western U.S., thus is a suitable tool for quantifying "episodic background" ozone. In this work, we use the AM3 base and NAB simulations at $\sim 200 \times 200$ km^2 horizontal resolution with 48 vertical levels from the surface to 0.01hPa, with the first model layer being ∼70 m-thick. The simulations use anthropogenic emissions from RCP8.5 [*Moss et al.*, 2010] and biomass burning emissions from GFED3 [*van der Werf et al.*, 2010] for 2010, as in *Lin et al.* [2013] (Lin, M., Horowitz L. W., Oltmans, S. J., Fiore, A. M. and Fan, S. 2013, Footprints of decadal climate variability in ozone at Mauna Loa Observatory, submitted to Nature Geoscience, 2013). AM3 applies climatological soil NO_x emissions, whereas biogenic isoprene emissions (based on MEGAN2.1) and lightning NO_x are tied

to the model meteorology [*Naik et al.*, 2013]. In the NAB simulation, North American anthropogenic emissions of non-methane ozone precursors and aerosols are set to zero.

2.4. GEOS-Chem adjoint

To estimate which specific species, sectors and locations most influence ozone and W126 in the U.S., we apply the GEOS-Chem adjoint model [*Henze et al.*, 2007] v34i. Adjoint modeling uses a computationally efficient approach for calculating sensitivities of an air quality metric J (e.g., mean concentration) to a set of input parameters of the chemical transport model such as emissions [*e.g.*, *Giering and Kaminski*, 1998; *Sandu et al.*, 2005; *Hakami et al.*, 2006]. The adjoint model of GEOS-Chem has been previously used for O_3 source-receptor modeling [*e.g.*, *Zhang et al.*, 2009a; *Walker et al.*, 2012; *Parrington et al.*, 2012]. The adjoint model calculates the influence of emissions (or other parameters) on variations in the cost function as normalized adjoint sensitivities, $\lambda_{E_{i,m}}$:

$$\lambda_{E_{i,m}} = \frac{\partial J}{\partial E_{i,m}} \frac{E_{i,m}}{J} \tag{2}$$

These sensitivities represent a fractional change in the cost function J to a fractional change in emissions E of source m in location i, and are calculated about the current model state. For sensitivity analysis in this work, J is defined as either the average 3-month cumulative W126 or daytime ozone over the continental U.S., as described in Section 3.3.3 and Table 1. For W126 this can be expressed as

$$J = \frac{1}{N} \sum_{i}^{N} \sum_{k}^{M} DI_{i,k} \tag{3}$$

where $DI_{i,k}$ is a daily W126 index in location i on day k, M is a number of days (i.e., 92) and N is a number of locations. Adjoint simulations are performed separately for each

month, with sensitivities integrated backward in time for one month preceding the month in which the cost function is evaluated. This is done in order to fully account for the influence of emissions of ozone precursors. To obtain the 3-month normalized sensitivities discussed in this work, the sum of normalized sensitivities scaled by each month's cost function is divided by the sum of J over 3 months. For further interpretation, sensitivity results are grouped by location, species and emission sectors.

3. Results and discussion

3.1. Observed W126 in 2010

Figure 3 presents time series of the annual observed 3-month W126 index in the continental U.S. and three regions (California, intermountain West and Atlantic) plotted in Figure 2a. The mean W126 values for each region (solid lines) are obtained by averaging the maximum 3-month sums across all monitoring stations within the region. This 3-month period varies from station to station and is typically between April and September. For comparison, the means obtained by averaging the 3-month sum for May–June–July, i.e., with the period fixed across all stations, are plotted with dashed lines, and are lower than the means obtained for the "true" W126 season for each year and station, as expected. The difference is especially large for California in 2010, where the ozone season varies widely based on location and the maximum W126 values were reached in June-July-August, on average. The highest 3-month W126 values are found in the California region during all five years. There is a significant degree of interannual variability for all regions with the overall decreasing trend. All regions except California exhibit a minimum in 2009, which was a low-ozone year across the U.S. [*CASTNET 2009 report*, 2011]. The second lowest 3-month W126 in the U.S. occurred in 2010, at least partially

due to the unusually wet conditions in spring and summer of 2010 according to the NOAA National Climatic Data Center (see http://www.ncdc.noaa.gov/temp-and-precip/).

3.2. Model performance for daytime ozone and W126

We first compare base case simulations to observations. Figure 2 shows the 3-month mean of the observed daytime ozone from CASTNET and AQS and corresponding estimates from each model. The highest average daytime ozone is observed in California and in the mountain sites in the West. The spatial distribution of daytime ozone varies among the models. This is due to the differences in their meteorology, stratospheric influences, chemistry (such as the treatment of isoprene nitrates) and emissions (Table 2). A large overestimation of daytime ozone in the eastern U.S. is apparent in all models. STEM over-predicts O_3 levels in the Iowa-Kansas-Oklahoma area. This bias is likely to be associated with meteorological fields and representation of land surface characteristics that affect physical processes as well as biogenic emissions in the model.

The W126 index exhibits spatial patterns similar to daytime ozone (Figure 4), but with the regions of low and high ozone greatly emphasized due to the sigmoidal weighting of the W126 function. Even though the May–July W126 index does not always correspond to the maximum 3-month W126 sum for analyzed locations, a number of sites experience W126 levels exceeding those that have been considered for the secondary standard (7–15 ppm-hours) during this period. The maximum W126 index of 45 ppm hours is observed in San Bernardino County, California. California exhibits the strongest W126 gradients; models are known to have difficulties reproducing spatial features of ozone in this region due to complex topography and failure to simulate ventilation of coastal pollution [*e.g.*, *Fiore et al.*, 2002]. STEM and GEOS-Chem are able to resolve more spatial features in daytime

ozone in this region compared to the coarse-grid AM3 simulation. Model resolution is especially important for the W126 metric as it exhibits sharper spatial gradients compared to the mean daytime ozone. Observed W126 is also high in the eastern part of the country (up to 25 ppm hours) where the models tend to overestimate W126 by a factor of two to four.

We also evaluate the daily time series of the mean daytime ozone and W126 daily index in each study domain, see Figure 5. Each model was first sampled at its native resolution at the time and location of observations followed by spatial averaging on a daily basis over the monitoring sites within the region. The three-model mean and standard deviation were then calculated based on model daily means for the region. Table 3 summarizes the regional 3-month means and temporal correlation coefficients between the observed and simulated daily values for individual models and for three-model means. The NAB values estimated for both daytime ozone and the W126 daily index are also given. The models reproduce day-to-day variability in the daytime ozone and W126 daily index well, with the exception of AM3 in California ($r = 0.47$ for ozone and $r = 0.22$ for W126), where AM3 also has a positive bias of $\sim$10 ppbv. *Lin et al.* [2012b] and *Lin et al.* [2012a] previously reported high bias in the 50×50 km AM3 simulations for April–June 2010 in the western U.S., which they attributed to the combined influence from missing O_3 sinks and model limitations in resolving mesoscale meteorology. We could not use the 50×50 km AM3 simulations in this analysis, as results for July 2010 were not available. However, comparing the nested and coarse GEOS-Chem results suggests that using the coarser AM3 simulations may not significantly affect the model's ability to represent large-scale patterns. For GEOS-Chem, we found that while the fine resolution improved the

representation of spatial patterns, especially in California, the choice of resolution did not affect the ability to simulate day-to-day variability in ozone and W126 over the study regions.

The three-model ozone mean (red line in Figure 5) overestimates the observations (black) over the Atlantic region on a daily basis by ∼15 ppbv. The bias in daily W126 (and, subsequently, the 3-month index) appears to result from persistent bias in daytime ozone (as opposed to being driven by a few large events). Additionally, model performance for W126 is worse than for the mean daytime ozone because of disproportionate sensitivity to model errors at the high end of the ozone concentration range [*Tong et al.*, 2009; *Holloway et al.*, 2012]. This effect also leads to degraded correlation between observations and models compared to daytime ozone (Table 3). Using the reduced major axis (or RMA) two-sided regression technique [*Ayers*, 2001; *Draper and Smith*, 1998] for the three-model mean in the Atlantic region we obtain the RMA slope of 1.9 and intercept of 159 ppbv hours for W126 ($r = 0.71$), while simulations in California and the intermountain West are relatively unbiased (slope of 1.1 and intercept of 3 ppbv hours, $r = 0.66$, and slope of 0.92 and intercept of 58 ppbv hours, $r = 0.69$, respectively).

Bias of >10 ppbv in the eastern U.S. in summer is a well-known issue for chemical transport models [*Fiore et al.*, 2009; *Reidmiller et al.*, 2009]. Positive biases of 9–20 ppbv have been found for MDA8 ozone in that region in the multi-model HTAP study of *Reidmiller et al.* [2009] in summer 2001. Recent analysis of *Zhang et al.* [2011] presented a rather unbiased GEOS-Chem analysis for spring and summer of 2006, which can be at least partially explained by the difference between the years modeled, with 2010 being a significantly lower-ozone year compared to 2006 (e.g., Figure 3). GEOS-Chem reproduces

well the total amount of precipitation in May–July 2010 compared to the NADP NTN observations (available at http://nadp.sws.uiuc.edu), hence it is unlikely that the bias is caused by missing precipitation events, even though conditions in some northeastern states were unusually wet. We find that when we decrease U.S. NO_x emissions by 30% in GEOS-Chem ozone levels are reduced by 5 ppbv on average, implying that some of the model bias could be due to relatively recent emission reductions that are not reflected in the emission inventories used [*e.g.*, *Russell et al.*, 2012]. There is also indication that GEOS-Chem routinely under predicts ozone dry deposition in the northeastern U.S., which may also contribute to the high ozone bias in that region (Dylan Jones, personal communication, 2013). The bias in GEOS-Chem would be further enhanced, with the largest increases of up to 5 ppbv in the southeastern U.S., if we updated the isoprene nitrate yield to 10%. The impact of model bias on the source apportionment in this work is discussed in Section 3.3.3.

3.3. Source sensitivity analysis

3.3.1. Modeled ozone and W126 North American Background

The spatial distribution of the NAB and its percent contribution to daytime ozone from each model is shown in Figure 6. The results are similar to the estimates reported previously for similar ozone metrics in spring–summer [*Fiore et al.*, 2003; *Zhang et al.*, 2011; *Emery et al.*, 2012], with the highest values occurring in the western U.S. We took the ratio of the U.S.-averaged NAB to the base case result for each model and found a range of 56–67% for the NAB contribution to the 3-month mean daytime ozone for three CTMs. For the intermountain West region this range is 64–78%. For individual locations the NAB contributions vary between 30 and 80% for a May-June-July daytime

ozone mean. These numbers are within the range that can be estimated from *Fiore et al.* [2002], e.g., ∼40–70% for the mean afternoon ozone in 2001, and ∼70% for MDA8 at the intermountain West sites in summer of 2006 [*Zhang et al.*, 2011].

The magnitude of the NAB ozone varies significantly among the models, with NAB in STEM being ∼10 ppbv lower, on average, than NAB in GEOS-Chem, especially in the Atlantic and Intermountain West regions. Base case STEM ozone was higher than observed in these regions. Two main factors could have been responsible for the low NAB in STEM— emissions from natural sources and transported background ozone, i.e., ozone from the extra-regional contributions. Transported background ozone includes ozone and its precursors from the lower stratosphere and outside of North America and is important for NAB ozone in spring and summer [*Huang et al.*, 2010, 2013]. This background is included in the top and lateral boundary conditions used by STEM for both base and NAB simulations. However, in this work they are provided by GEOS-Chem, which has significantly higher NAB ozone than STEM, and, therefore the transported background cannot account for the difference between these two models. We conducted individual STEM sensitivity simulations for the base case where NA biogenic, biomass burning and lightning emissions were set to zero (not shown). The results indicate that surface ozone in the U.S. is most sensitive to biogenic emissions (soil NO_x and biogenic hydrocarbons), with sensitivities showing strong spatial and temporal variability. This implies that uncertainties in the biogenic emissions are of a greater importance than uncertainties in other NA natural sources.

Figure 7 shows the NAB estimate for the 3-month W126 metric. The three models predict low W126 values in the absence of North American anthropogenic emissions,

with most locations below 3 ppm-hours, well below levels considered for the W126-based secondary standard. NAB is less than 6% of the base-case W126 in the East and up to 35% in the West (Figure 7). The mean NAB values for W126 over the entire contiguous U.S. for the three models are in the range of 4–12% of total W126. For the intermountain West region, the mean W126 NAB value for the three models is in the range from 9–27%. These values are low compared to the NAB contribution to the mean daytime ozone and are due to the highly nonlinear W126 dependence on ozone, which results in W126 for the base case being significantly larger than the sum of W126 estimated from the background ozone and W126 estimated from the ozone produced from the North American anthropogenic sources. Thus, it is important to realize that even though the background contribution to the daytime ozone is high at some locations, the fact that W126 is extremely low in the absence of North American anthropogenic emissions emphasizes the importance of these emissions. It is only after their addition to the background that ozone levels become significant enough to yield high W126. Further discussion of the implications of non-linearity for source-attribution results in this work is given in Section 3.3.5.

Models differ on their predictions of the NAB behavior on the days with high W126 DI, with the largest disagreement in the intermountain West region. AM3 and GEOS-Chem estimate that most of the variability in the W126 DI in this region is controlled by NAB ($r = 0.91$ and $r = 0.73$ for AM3 and GEOS-Chem, respectively), while STEM predicts no temporal correlation between the total W126 and NAB. When a three-model mean is used, W126 DI NAB explains ∼30% ($r = 0.55$) of the daily variability in the W126 DI in the intermountain West, which is on the lower end of the range of 20–54% reported earlier for MDA8 at selected sites in the same region for spring and summer of 2006 [*Zhang et al.*,

2011]. As evident from Figure 5, the W126 NAB increases occasionally on days with high W126 daily index in the California region ($r = 0.23$, based on three-model mean) and there is no significant temporal correlation of NAB with the W126 DI in the Atlantic region where regional photochemical production is understood to be the most important contribution [*Fiore et al.*, 2003; *Zhang et al.*, 2011]. For each individual model there is a slight decrease in correlation between the NAB and W126 compared to correlation between the NAB and total daytime ozone. As NAB increases less than the total W126, no correlation is present between the NAB percent contribution and W126 for California and the intermountain West, and there is a weak negative correlation between the NAB percent contribution and W126 for the Atlantic region ($r = -0.42$), consistent with the findings of *Henderson et al.* [2012] for MDA8.

To determine the extent to which model bias could affect estimates for the 3-month W126 NAB contribution, we apply a simple bias correction, to GEOS-Chem results only, for the California and Atlantic regions. We picked these regions because of the differences in model performance and because they represent cases with high and low NAB. We first sample the models at the locations of observations and find the NAB contribution for each region using the model results only, e.g., $\frac{\sum_i W126_{NABi}}{\sum_i W126_{BASEi}} \times 100\%$, where i includes all GEOS-Chem grid cells containing at least one station in the region. We estimate these contributions to be 1.0% for the Atlantic region and 12.7% for the California region. Next we modify the expression above and apply the observation-based correction factors in each region to obtain the NAB contributions as follows:

$$\mathrm{NAB}\% = \sum_i \frac{W126_{NABi} \times \frac{W126_{OBSi}}{W126_{BASEi}}}{\sum_i W126_{OBSi}} \times 100\% \quad (4)$$

where $W126_{OBSi}$ is an observed value of W126 and $W126_{NABi}$ and $W126_{BASEi}$ are estimates of the base and NAB W126 values at location i, respectively. Applying correction factors to NAB estimates in this way assumes that model bias is uniform across the base and NAB runs. The new NAB contributions are 1.2 and 14.4%, thus the applied correction results only in minor changes to the original estimates, likely owing to the fact that most model bias is in the East, where NAB is low.

3.3.2. Impact of stratospheric ozone on W126

To investigate the stratospheric contribution to W126 levels we use AM3, which includes fully interactive stratospheric and tropospheric chemistry. The AM3 stratospheric ozone tracer, O_3S, is defined relative to a dynamically varying tropopause [*Prather et al.*, 2011] and is used to tag O_3 originating from the stratosphere. Through employing this technique with high-resolution (∼50×50 km) AM3 simulations, *Lin et al.* [2012b] have previously demonstrated that stratospheric intrusions can have a significant impact on MDA8, especially at high-elevation sites in springtime.

AM3 gives 3-month means of O_3S across the continental U.S. ranging from 4 to 17 ppbv (mean of 10 ppbv). Thus W126 estimated from O_3S directly is negligible (<2% of total W126, on average) due to the low weights given to O_3 less than 40 ppbv in the W126 function. The coarse horizontal resolution of the AM3 model in this work was insufficient for more detailed analysis to resolve the temporal and spatial variability of O_3S and its influence on W126.

3.3.3. Differentiating emission influences using adjoint sensitivities

We apply the adjoint of GEOS-Chem to derive the spatially-resolved first order normalized sensitivities of the nationwide 3-month average daytime ozone and 3-month W126

to the model's emissions. The adjoint analysis is performed for the base-case run (with unperturbed emissions) twice — first, with the cost function, J, defined as the 3-month W126 and, second, with J defined as the 3-month average daytime ozone, each averaged over the U.S. domain (Table 1). Due to computational expenses, the global-scale adjoint runs are performed at a horizontal resolution of $2^\circ \times 2.5^\circ$. While it is possible that this may limit our ability to resolve some smaller-scale processes, we find that the 3-month W126 metric obtained with this resolution is similar overall (i.e., an average difference of 0.7 ppm-hrs for the base case) to the results obtained with a resolution of $1/2^\circ \times 2/3^\circ$, used in the rest of this work (see Figures S2 and S3 in supporting information).

3.3.3.1. Base-case W126 contributions

The adjoint sensitivities can be understood in terms of a fractional change in J as a result of small fractional changes in emissions of the contributing species, such as NO_x and CO, at each location. For each species, adjoint sensitivities identify emissions contributing the most to J. The highest W126 sensitivity is to anthropogenic NO_x emissions within the U.S. (Figure 8a) with little influence from abroad. Sensitivities to anthropogenic CO are more spread out, with relatively high values over parts of China, Mexico and India (Figure 8b). While the magnitude of NO_x sensitivities in individual locations are >20 times higher than sensitivities to CO, on average, the total NO_x influence is higher only by a factor of 10 due to the fact that CO sensitivities are more widely distributed though out the Northern Hemisphere.

The sensitivities can be aggregated to assess total W126 influences from source categories, including countries of origin, emission sectors and emitted species. The sum of all normalized adjoint sensitivities for a function that is non-linear with respect to model

parameters can deviate from 100%, as is the case here (Section 3.3.5). In the discussion below we focus on the relative importance of emission sources and all adjoint sensitivities are normalized by the sum of the total. Figure 9 shows sensitivities of W126 to emissions aggregated by sectors: anthropogenic, biomass burning and natural, which includes isoprene emissions and NO_x emissions from lightning and soil. Soil emissions in the model include both the natural component as well as emissions from fertilized soil. However, fertilized emissions make a relatively small fraction of total soil emissions ($\sim$25%). The mean nationwide W126 is most sensitive to the anthropogenic (58%) and natural (25%) NO_x emissions, followed by NMVOCs (10%) and CO (7%). Eighty percent of the sensitivity to NO_x anthropogenic emissions is within the U.S., followed by emissions in Canada (9%), Mexico (4%) and China (3%). W126 is relatively insensitive to total isoprene (1.3% of the total sensitivity) compared to the rest of the NMVOCs because isoprene sensitivities can be both negative and positive depending on location. Isoprene leads to ozone production in the presence of elevated NO_x concentrations, as modeled in the northeastern U.S. This results in high positive sensitivities as seen in Figure 10. Isoprene also destroys ozone through direct ozonolysis in areas with low NO_x, as modeled in the southeastern U.S. The absolute magnitude of isoprene sensitivities in individual locations are, on average, $\sim$7 times lower than sensitivities to anthropogenic NO_x emissions. Sensitivities of ozone to isoprene emissions depend, among other parameters, on the isoprene nitrate yield and the fate of isoprene nitrates assumed in the model. W126 sensitivities are more negative in this work due to the high isoprene nitrate yield value and assumption that isoprene nitrates act as a terminal sink for NO_x. A one-month sensitivity run with the reduced isoprene nitrate yield (10%) exhibited enhanced positive isoprene sensitivities and weak-

ening of the negative ones. Sensitivities will become even more positive if partial NO_x recycling for isoprene nitrates is allowed [*Mao et al.*, 2013].

Figure 11 shows sensitivities to anthropogenic NO_x, CO and NMVOC emissions for W126 and daytime ozone aggregated by country. As the importance of the long-range transport of pollution relative to the local sources is determined by a species' lifetime, a greater fraction of CO influences are from remote regions for both W126 and ozone sensitivities, compared to NO_x. Thus, GEOS-Chem indicates that China is the next most important W126 source region for CO (15%) after the U.S. (56%). Emission influences for daytime ozone are overall similar to the influences for the W126 metric, but with W126 being relatively less sensitive to long-range transport. This is due to the strong dependence of W126 on high ozone concentrations, which are typically observed in stagnant conditions when local emission sources play a dominant role [*e.g.*, *Fiore et al.*, 2003].

The adjoint sensitivities discussed above correspond to the base case state and are not expected to change significantly with moderate changes in emissions, as was shown for the episode-averaged 8-hour ozone by *Cohan et al.* [2005]. To assess the degree to which sensitivities in different locations are influenced by emissions in other locations (i.e., second-order cross-sensitivity), we performed additional runs with emissions perturbed (halved or doubled) on a country or on a grid-scale basis. We find that sensitivities to U.S. emissions decreased by 63% when U.S. emissions were halved, implying that the same fractional change in emissions will result in the W126 relative response which is 63% lower than the W126 response for the base case. This change did not affect the fraction of response to change in U.S. emissions relative to change in emissions in other countries. These sensitivities were not affected significantly by changes in emissions outside of the U.S. (i.e., $< 5\%$

when emissions in either Canada, Mexico or China were halved or doubled). Sensitivities to emissions outside of the U.S. do not exhibit significant inter-dependence, i.e., doubling or halving emissions in Mexico has a relatively minor impact on the sensitivities of W126 to emissions in China ($< 8\%$) and in Canada ($< 2\%$). For single grid-cell perturbations outside the U.S. the W126 response was approximately linear implying that individual remote adjoint sensitivities can be used for a relatively accurate prediction of the resulting change. These results imply that the emission sensitivities obtained in this work for different regions are robust to emissions changes (or uncertainties in emission inventories) in other regions.

3.3.3.2. NAB contributions

To learn about emission sources contributing to the W126 NAB in the U.S. we can use the adjoint sensitivities obtained for the base run, but include only sensitivities to emissions considered as part of the NA background, i.e., emissions from natural sources and anthropogenic emissions from outside NA. The alternative approach is to run the adjoint simulation with NA anthropogenic emissions set to zero. We find that both approaches provide similar results, with the main difference being that in the absence of the NA anthropogenic emissions the changes in chemical regime lead to an estimated negative isoprene response, except in a few localized areas with active biomass burning. Here we present the results for the base adjoint run, as information on natural sources influencing W126 at the present conditions is more relevant compared to the hypothetical NAB case. The main W126 sensitivities are to NO_x emissions (79.8% of the total), followed by CO (9.2%), NMVOCs (7.3%) and isoprene influence of 3.6% (results normalized), with NO_x emissions from lightning and soil dominating the total NO_x influences (Figure 12).

Long-range transport of anthropogenic NO_x emissions from outside NA plays a lesser role, with biomass burning NO_x having the least impact. The spatial distributions of these emissions and their sensitivities are very different (Figure 13). Thus, more than one-third of the influence from lightning NO_x comes from outside of North America (40%), while for soil emissions it is <7%. The average W126 sensitivity (%) per unit NO_x emitted is highest for lightning emissions because this NO_x is generally emitted in more pristine conditions where ozone production efficiency is higher. Anthropogenic NO_x from outside North America has the lowest % sensitivity per fraction of total NO_x emitted, and the total impact of these emissions declines later in the summer, consistent with the seasonality of the impact of Asian emissions on North America [*Liu et al.*, 2003]. The fire activity during May–July 2010 was relatively low (http://www.ncdc.noaa.gov/sotc/fire). NO_x from fires is likely to have a higher contribution in high-fire years, especially in the western U.S. [*Mueller and Mallard*, 2011; *Jaffe*, 2011].

3.3.4. Effect of bias-correction on source attribution results

Adjoint sensitivities are only as accurate as the GEOS-Chem representation of the processes influencing ozone and W126 are. To determine how GEOS-Chem model bias affects the W126 sensitivity results, we repeat the adjoint analysis with observation-based scaling factors applied to minimize model errors. In this new adjoint run, J is defined only over model cells with existing observations and the scaling factors at each location represent the ratio of the observed to modeled W126 value in that grid cell, $W126_{obs,i}$ and $W126_{mod,i}$, respectively:

$$J = \frac{1}{N}\sum_{i}^{N}\sum_{k}^{M} DI_{i,k} \times \frac{W126_{obs,i}}{W126_{mod,i}} \quad (5)$$

We exclude $\sim$ 30% of cells in the continental U.S. due to lack of observations. The bias correction results in reduction of adjoint sensitivities mostly over the areas with W126 overestimation, such as the Atlantic region and Gulf Coast, and increased sensitivities over areas in California, the southeastern U.S. and parts of the West. However the corrected sensitivities have only a minor (<3%) effect for the percentages of total sensitivity aggregated by species, sector or country, consistent with the bias-correction results presented in Section 3.3.1.

3.3.5. Comparison of source analysis methods

It is important to distinguish between the results of source analysis quantified by setting emissions to zero and the results obtained by using a smaller change in emissions, e.g. 20%, or from adjoint results that project responses from an infinitesimally small source perturbation. While the first approach measures the minimum obtainable level of an ozone metric in the absence of emission sources, the latter predicts the metric's response due to marginal changes in emissions. In the case of nonlinear dependence of the metric on emission sources, linear scaling of the first-order sensitivities to infer a response from a large perturbation will be subject to truncation errors. To assess the behavior of W126 in response to incremental changes in precursor emissions, we perform an additional GEOS-Chem simulation with the North American anthropogenic sources reduced by 20%. We find that the mean daytime ozone had a greater response to the 100% reduction (38%) compared to the response estimated by scaling up the response to a 20% reduction (5×4.4%=22%), consistent with previous work [*Wu et al.*, 2009; *Wild et al.*, 2012]. This is due to the fact that the daytime ozone concentrations have a nonlinear dependence on NO_x emissions, which can be represented by a concave function [*Lin*

et al., 1988], with ozone becoming more sensitive to the remaining NO_x as emissions are reduced. For the 3-month W126 index this response is reversed (92% W126 reduction if all NA emissions set to zero versus 113% obtained by scaling up the response to a 20% perturbation) due to the convex dependence of W126 on ozone concentrations in the range considered. As illustrated in Figure 14, extrapolation of the adjoint sensitivities to a 100% perturbation results in overestimated contribution of emissions for W126 and underestimated contribution for daytime ozone, similar to the case with 20% perturbation. The adjoint results presented in this plot are obtained by summing up the normalized sensitivities for all species from anthropogenic sources across North America, thus obtaining 24% of J for daytime ozone and 156% for W126. While aggregated marginal sensitivities should not be used to infer absolute contributions of emission sources to the air quality metric for the case when the relationship is non-linear, they provide a valuable insight into the metric's response to small emission changes in a relatively unperturbed environment. For example, the adjoint method indicates that a 10% reduction in NA anthropogenic emissions will decrease the 3-month daytime ozone by 2.4% and W126 by 15.6%. As was mentioned earlier, adjoint sensitivities are also more accurate when used on a grid-cell basis to provide the metric's response to single grid-cell perturbations outside of the U.S.

4. Conclusions

We present model results from three CTMs to evaluate model abilities to simulate the W126 ozone metric in the U.S. and to quantify the contribution of emission sources to this metric. All models overestimate daytime ozone over the eastern U.S. on a daily-basis, by ~15ppbv. This high bias is further exacerbated by nonlinear weighting for the W126 index leading to an overestimation of the 3-month W126 by a factor of two to four in this

region. In contrast, models are relatively unbiased over the California and intermountain West regions. Simulating the W126 metric in these regions is arguably of greater value from a modeling standpoint for several reasons. First, compared to the eastern U.S., the West contains the largest NAB levels. Secondly, much of the West is relatively sparsely monitored from the point of view of vegetative exposure, with existing monitor locations designed around primary ozone standards. Lastly, of the counties presently monitored, a greater potential for disconnect between attaining primary versus W126-based ozone standards has been demonstrated in the West [*U.S. EPA*, 2011]. We find significant differences in estimates of the W126 North American background among the participating models. Therefore, the use of multiple models is crucial in assessing the W126 levels in the absence or reduction of North American anthropogenic emissions. Based on a three-model mean, NAB explains ∼30% of the day-to-day variability in the W126 daily index in the intermountain West. NAB increases only occasionally on days with high W126 daily index in the California region ($r = 0.23$) and there is no significant correlation of NAB with the W126 DI in the Atlantic region. We find the issue of resolution especially important for the models' ability to reproduce the sharp spatial gradients of W126, particularly in California. The total NAB contribution to daytime ozone is 56–67%, as based on three models, and is 64–78% for the intermountain West. However, due to the highly-nonlinear dependence of W126 on ozone, W126 in the absence of NA anthropogenic emissions is estimated to be only 4–12% of the base levels for the contiguous U.S. and is in the range from 9–27% for the intermountain West region. The highest NAB contribution is found in the West where the W126 NAB can be up to 35% of current levels.

To investigate the sources influencing W126 in the U.S. we perform sensitivity analysis using the GEOS-Chem adjoint model, which shows that W126 is most sensitive to the anthropogenic (58%) and natural (25%) NO_x emissions, followed by NMVOCs (10%) and CO (7%). Eighty percent of sensitivity to the NO_x anthropogenic emissions is within the U.S., followed by emissions in Canada (9%), Mexico (4%) and China (3%). The NAB component of W126 in the U.S. is most sensitive to natural NO_x sources, with lightning and soil being most important. It is important to note that the NAB contribution is expected to vary with the 3-month season, and the impact of long-range transport or stratospheric intrusions can be higher if the analyzed period includes April or March.

This work is the first national-scale source attribution analysis for W126 and shows that long-range transport of pollution has a minor impact on this metric in the U.S. and that domestic emissions reductions should be effective in lowering W126 levels. While the adjoint sensitivities are determined for the nationwide W126, this analysis targets the areas with the most ozone damage because of the W126 weighting which emphasizes the highest ozone concentrations. It is important to note that the modeled NAB and adjoint sensitivities are only as accurate as the model representation of W126 and the emissions driving the simulations. Further research is needed to improve the models' performance in the eastern U.S., where most models overestimate surface ozone concentrations. The bias-correction analysis shows that the conclusions based on aggregated adjoint emission sensitivities in this work are not significantly affected by model bias or uncertainties in emission inventories, including the impact of emission uncertainties in one country on sensitivities to emissions in another. Use of the adjoint sensitivities to investigate sources contributing to regional or county-scale average W126, however, will require observation-

based bias correction which is subject to availability of ozone measurements. This can be problematic in the high-W126 areas in the rural West, where the monitoring network is currently limited. Future modeling studies will be of value for estimating exposure in areas with limited monitoring.

Future work should expand this analysis by performing source attribution of ozone damage by vegetation and crop type. As the W126 seasonality and NAB levels depend upon location, next steps will focus on a finer spatial scale with study regions chosen based on their W126 levels or based on having high value for the public (e.g., national parks with ozone-sensitive vegetation). As emissions reductions take place as a result of implementing the primary ozone standard, source assessment for W126 will need to be re-evaluated.

Acknowledgments. We thank Victoria Sandiford (EPA/OAQPS), Jeffrey D. Herrick (EPA/ORD), J. Travis Smith (EPA/OAQPS) and Ellen Porter (NPS/ARD) for valuable discussion. This work was supported by NASA Air Quality Applied Sciences Team award NNX11AI54G.

References

Adhikary, B., G. R. Carmichael, S. Kulkarni, C. Wei, Y. Tang, A. D'Allura, M. Mena-Carrasco, D. G. Streets, Q. Zhang, R. B. Pierce, J. A. Al-Saadi, L. K. Emmons, G. G. Pfister, M. A. Avery, J. D. Barrick, D. R. Blake, W. H. Brune, R. C. Cohen, J. E. Dibb, A. Fried, B. G. Heikes, L. G. Huey, D. W. O'Sullivan, G. W. Sachse, R. E. Shetter, H. B. Singh, T. L. Campos, C. A. Cantrell, F. M. Flocke, E. J. Dunlea, J. L. Jimenez, A. J. Weinheimer, J. D. Crounse, P. O. Wennberg, J. J. Schauer, E. A. Stone, D. A.

Jaffe, and D. R. Reidmiller (2010), A regional scale modeling analysis of aerosol and trace gas distributions over the eastern Pacific during the INTEX-B field campaign, *Atmos. Chem. Phys.*, *10*(5), 2091–2115, doi:10.5194/acp-10-2091-2010.

Allen, D. J., K. E. Pickering, R. W. Pinder, B. H. Henderson, K. W. Appel, and A. Prados (2012), Impact of lightning-NO on eastern United States photochemistry during the summer of 2006 as determined using the CMAQ model, *Atmos. Chem. Phys.*, *12*(4), 1737–1758, doi:10.5194/acp-12-1737-2012.

Arbaugh, M. J., P. R. Miller, J. J. Carroll, B. Takemoto, and T. Procter (1998), Relationships of ozone exposure to pine injury in the Sierra Nevada and San Bernardino Mountains of California, USA, *Environ. Pol.*, *101*(2), 291 – 301, doi: http://dx.doi.org/10.1016/S0269-7491(98)00027-X.

Avnery, S., D. L. Mauzerall, J. Liu, and L. W. Horowitz (2011), Global crop yield reductions due to surface ozone exposure: 1. year 2000 crop production losses and economic damage, *Atmos. Environ.*, *45*(13), 2284 – 2296, doi: http://dx.doi.org/10.1016/j.atmosenv.2010.11.045.

Avnery, S., D. L. Mauzerall, and A. M. Fiore (2013), Increasing global agricultural production by reducing ozone damages via methane emission controls and ozone-resistant cultivar selection, *Global Change Biology*, *19*(4), 1285–1299, doi:10.1111/gcb.12118.

Ayers, G. (2001), Comment on regression analysis of air quality data, *Atmos. Environ.*, *35*, 2423–2425.

Brown-Steiner, B., and P. Hess (2011), Asian influence on surface ozone in the United States: A comparison of chemistry, seasonality, and transport mechanisms, *J. Geophys. Res.*, *116*(D17), doi:10.1029/2011JD015846.

Carmichael, G. R., Y. Tang, G. Kurata, I. Uno, D. G. Streets, N. Thongboonchoo, J.-H. Woo, S. Guttikunda, A. White, T. Wang, D. R. Blake, E. Atlas, A. Fried, B. Potter, M. A. Avery, G. W. Sachse, S. T. Sandholm, Y. Kondo, R. W. Talbot, A. Bandy, D. Thorton, and A. D. Clarke (2003), Evaluating regional emission estimates using the TRACE-P observations, *J. Geophys. Res.*, *108*(D21), doi:10.1029/2002JD003116.

Carter, W. P. L. (2000), Documentation of the SAPRC-99 chemical mechanism for VOC reactivity assessment, final report to California Air Resources Board, Contract no. 92-329 and 95-308.

CASTNET 2009 report (2011), Clean Air Status and Trends Network (CASTNET) 2009 annual report (EPA Contract No. EP-W-09-028), prepared by: MACTEC Engineering and Consulting, Inc.

Chappelka, A., J. Skelly, G. Somers, J. Renfro, and E. Hildebrand (1999), Mature black cherry used as a bioindicator of ozone injury, *Water, Air, and Soil Pollution*, *116*(1-2), 261–266, doi:10.1023/A:1005260422738.

Cohan, D. S., A. Hakami, Y. Hu, and A. G. Russell (2005), Nonlinear response of ozone to emissions: Source apportionment and sensitivity analysis, *Environ. Sci. Technol.*, *39*(17), 6739–6748, doi:10.1021/es048664m, pMID: 16190234.

Draper, N. R., and H. Smith (1998), *Applied Regression Analysis*, 706 pp., John Wiley & Sons, Inc.

Emery, C., J. Jung, N. Downey, J. Johnson, M. Jimenez, G. Yarwood, and R. Morris (2012), Regional and global modeling estimates of policy relevant background ozone over the United States, *Atmos. Environ.*, *47*, 206 – 217, doi:10.1016/j.atmosenv.2011.11.012.

Fiore, A., D. J. Jacob, H. Liu, R. M. Yantosca, T. D. Fairlie, and Q. Li (2003), Variability in surface ozone background over the United States: Implications for air quality policy, *J. Geophys. Res.*, *108*(D24), doi:10.1029/2003JD003855.

Fiore, A. M., D. J. Jacob, I. Bey, R. M. Yantosca, B. D. Field, A. C. Fusco, and J. G. Wilkinson (2002), Background ozone over the United States in summer: Origin, trend, and contribution to pollution episodes, *J. Geophys. Res.*, *107*(D15), ACH 11–1–ACH 11–25, doi:10.1029/2001JD000982.

Fiore, A. M., F. J. Dentener, O. Wild, C. Cuvelier, M. G. Schultz, P. Hess, C. Textor, M. Schulz, R. M. Doherty, L. W. Horowitz, I. A. MacKenzie, M. G. Sanderson, D. T. Shindell, D. S. Stevenson, S. Szopa, R. Van Dingenen, G. Zeng, C. Atherton, D. Bergmann, I. Bey, G. Carmichael, W. J. Collins, B. N. Duncan, G. Faluvegi, G. Folberth, M. Gauss, S. Gong, D. Hauglustaine, T. Holloway, I. S. A. Isaksen, D. J. Jacob, J. E. Jonson, J. W. Kaminski, T. J. Keating, A. Lupu, E. Marmer, V. Montanaro, R. J. Park, G. Pitari, K. J. Pringle, J. A. Pyle, S. Schroeder, M. G. Vivanco, P. Wind, G. Wojcik, S. Wu, and A. Zuber (2009), Multimodel estimates of intercontinental source-receptor relationships for ozone pollution, *J. Geophys. Res.*, *114*(D4), doi:10.1029/2008JD010816.

Giering, R., and T. Kaminski (1998), Recipes for adjoint code construction, *ACM Trans. Math. Softw.*, *24*(4), 437–474, doi:10.1145/293686.293695.

Guenther, A., T. Karl, P. Harley, C. Wiedinmyer, P. I. Palmer, and C. Geron (2006), Estimates of global terrestrial isoprene emissions using megan (model of emissions of gases and aerosols from nature), *Atmos. Chem. Phys.*, *6*(11), 3181–3210.

Guenther, A. B., X. Jiang, C. L. Heald, T. Sakulyanontvittaya, T. Duhl, L. K. Emmons, and X. Wang (2012), The Model of Emissions of Gases and Aerosols from Nature version 2.1 (MEGAN2.1): an extended and updated framework for modeling biogenic emissions, *Geosci. Model Dev.*, *5*(6), 1471–1492, doi:10.5194/gmd-5-1471-2012.

Hakami, A., J. H. Seinfeld, T. Chai, Y. Tang, G. R. Carmichael, and A. Sandu (2006), Adjoint sensitivity analysis of ozone nonattainment over the continental United States, *Environ. Sci. Technol.*, *40*(12), 3855–3864, doi:10.1021/es052135g.

Henderson, B., N. Possiel, F. Akhtar, and H. Simon (2012), Regional and seasonal analysis of North American background ozone estimates from two studies, Prepared for Ozone NAAQS Review Docket EPA-HQ-OAR-2012-0699, Aug 2012, Available at: http://www.epa.gov/ttn/naaqs/standards/ozone/s_o3_td.html.

Henze, D. K., A. Hakami, and J. H. Seinfeld (2007), Development of the adjoint of GEOS-Chem, *Atmos. Chem. Phys.*, *7*(9), 2413–2433, doi:10.5194/acp-7-2413-2007.

Hollaway, M. J., S. R. Arnold, A. J. Challinor, and L. D. Emberson (2012), Intercontinental trans-boundary contributions to ozone-induced crop yield losses in the Northern Hemisphere, *Biogeosciences*, *9*(1), 271–292, doi:10.5194/bg-9-271-2012.

Huang, M., G. R. Carmichael, B. Adhikary, S. N. Spak, S. Kulkarni, Y. F. Cheng, C. Wei, Y. Tang, D. D. Parrish, S. J. Oltmans, A. D'Allura, A. Kaduwela, C. Cai, A. J. Weinheimer, M. Wong, R. B. Pierce, J. A. Al-Saadi, D. G. Streets, and Q. Zhang (2010), Impacts of transported background ozone on California air quality during the ARCTAS-CARB period — a multi-scale modeling study, *Atmos. Chem. Phys.*, *10*(14), 6947–6968, doi:10.5194/acp-10-6947-2010.

Huang, M., G. R. Carmichael, T. Chai, R. B. Pierce, S. J. Oltmans, D. A. Jaffe, K. W. Bowman, A. Kaduwela, C. Cai, S. N. Spak, A. J. Weinheimer, L. G. Huey, and G. S. Diskin (2013), Impacts of transported background pollutants on summertime western US air quality: model evaluation, sensitivity analysis and data assimilation, *Atmos. Chem. Phys.*, *13*(1), 359–391, doi:10.5194/acp-13-359-2013.

Jacob, D. J., J. A. Logan, and P. P. Murti (1999), Effect of rising asian emissions on surface ozone in the United States, *Geophys. Res. Lett.*, *26*(14), 2175–2178, doi:10.1029/1999GL900450.

Jaffe, D. (2011), Relationship between surface and free tropospheric ozone in the Western U.S., *Environ. Sci. Technol.*, *45*(2), 432–438, doi:10.1021/es1028102.

Kuhns, H., E. M. Knipping, and J. M. Vukovich (2005), Development of a United States-Mexico emissions inventory for the Big Bend Regional Aerosol and Visibility Observational (BRAVO) study, *J. Air Waste Manage. Assoc.*, *55*, 677–692.

Lefohn, A., and V. Runeckles (1987), Establishing a standard to protect vegetation—ozone exposure/dose considerations, *Atmos. Environ.*, (21), 561–568.

Lefohn, A., J. Lawrence, and R. Kohut (1988), A comparison of indices that describe the relationship between exposure to ozone and reduction in the yield of agricultural crops, *Atmos. Environ.*, (22), 1229–1240.

Lin, M., A. M. Fiore, L. W. Horowitz, O. R. Cooper, V. Naik, J. Holloway, B. J. Johnson, A. M. Middlebrook, S. J. Oltmans, I. B. Pollack, T. B. Ryerson, J. X. Warner, C. Wiedinmyer, J. Wilson, and B. Wyman (2012a), Transport of Asian ozone pollution into surface air over the western United States in spring, *J. Geophys. Res.*, *117*(D4), doi:10.1029/2011JD016961.

Lin, M., A. M. Fiore, O. R. Cooper, L. W. Horowitz, A. O. Langford, H. Levy, B. J. Johnson, V. Naik, S. J. Oltmans, and C. J. Senff (2012b), Springtime high surface ozone events over the western United States: Quantifying the role of stratospheric intrusions, *J. Geophys. Res.*, *117*(D19), doi:10.1029/2012JD018151.

Lin, X., M. Trainer, and S. C. Liu (1988), On the nonlinearity of the tropospheric ozone production, *J. Geophys. Res.*, *93*(D12), 15,879–15,888, doi:10.1029/JD093iD12p15879.

Liu, H., D. J. Jacob, I. Bey, R. M. Yantosca, B. N. Duncan, and G. W. Sachse (2003), Transport pathways for Asian pollution outflow over the Pacific: Interannual and seasonal variations, *J. Geophys. Res.*, *108*(D20), doi:10.1029/2002JD003102.

Mao, J., F. Paulot, D. J. Jacob, R. C. Cohen, J. D. Crounse, P. O. Wennberg, C. A. Keller, R. C. Hudman, M. P. Barkley, and L. W. Horowitz (2013), Ozone and organic nitrates over the eastern United States: Sensitivity to isoprene chemistry, *J. Geophys. Res.*, *118*(19), 11,256–11,268, doi:10.1002/jgrd.50817.

McDonald-Buller, E. C., D. T. Allen, N. Brown, D. J. Jacob, D. Jaffe, C. E. Kolb, A. S. Lefohn, S. Oltmans, D. D. Parrish, G. Yarwood, and L. Zhang (2011), Establishing policy relevant background (PRB) ozone concentrations in the United States, *Environ. Sci. Technol.*, *45*(22), 9484–9497, doi:10.1021/es2022818.

McLinden, C. A., S. C. Olsen, B. Hannegan, O. Wild, M. J. Prather, and J. Sundet (2000), Stratospheric ozone in 3-D models: A simple chemistry and the cross-tropopause flux, *J. Geophys. Res.*, *105*(D11), 14,653–14,665, doi:10.1029/2000JD900124.

Moss, R. H., J. A. Edmonds, K. A. Hibbard, M. R. Manning, S. K. Rose, D. P. van Vuuren, T. R. Carter, S. Emori, M. Kainuma, T. Kram, G. A. Meehl, J. F. B. Mitchell, N. Nakicenovic, K. Riahi, S. J. Smith, R. J. Stouffer, A. M. Thomson, J. P. Weyant,

and T. J. Wilbanks (2010), The next generation of scenarios for climate change research and assessment, *Nature*, *437*, 747–756, doi:10.1038/nature08823.

Mueller, S. F., and J. W. Mallard (2011), Contributions of natural emissions to ozone and PM2.5 as simulated by the Community Multiscale Air Quality (CMAQ) model, *Environ. Sci. Technol.*, *45*(11), 4817–4823, doi:10.1021/es103645m.

Murray, L. T., D. J. Jacob, J. A. Logan, R. C. Hudman, and W. J. Koshak (2012), Optimized regional and interannual variability of lightning in a global chemical transport model constrained by LIS/OTD satellite data, *J. Geophys. Res.*, *117*(D20), doi:10.1029/2012JD017934.

Naik, V., L. W. Horowitz, A. M. Fiore, P. Ginoux, J. Mao, A. M. Aghedo, and H. Levy (2013), Impact of preindustrial to present-day changes in short-lived pollutant emissions on atmospheric composition and climate forcing, *J. Geophys. Res.*, *118*(14), 8086–8110, doi:10.1002/jgrd.50608.

Ott, L. E., K. E. Pickering, G. L. Stenchikov, D. J. Allen, A. J. DeCaria, B. Ridley, R.-F. Lin, S. Lang, and W.-K. Tao (2010), Production of lightning NOx and its vertical distribution calculated from three-dimensional cloud-scale chemical transport model simulations, *J. Geophys. Res.*, *115*(D4), doi:10.1029/2009JD011880.

Parrington, M., P. I. Palmer, D. K. Henze, D. W. Tarasick, E. J. Hyer, R. C. Owen, D. Helmig, C. Clerbaux, K. W. Bowman, M. N. Deeter, E. M. Barratt, P.-F. Coheur, D. Hurtmans, Z. Jiang, M. George, and J. R. Worden (2012), The influence of boreal biomass burning emissions on the distribution of tropospheric ozone over North America and the North Atlantic during 2010, *Atmos. Chem. Phys.*, *12*(4), 2077–2098, doi:10.5194/acp-12-2077-2012.

Prather, M. J., X. Zhu, Q. Tang, J. Hsu, and J. L. Neu (2011), An atmospheric chemist in search of the tropopause, *J. Geophys. Res.*, *116*(D4), doi:10.1029/2010JD014939.

Reich, P. B., and R. G. Amundson (1985), Ambient levels of ozone reduce net photosynthesis in tree and crop species, *Science*, *230*(4725), 566–570, doi: 10.1126/science.230.4725.566.

Reidmiller, D. R., A. M. Fiore, D. A. Jaffe, D. Bergmann, C. Cuvelier, F. J. Dentener, B. N. Duncan, G. Folberth, M. Gauss, S. Gong, P. Hess, J. E. Jonson, T. Keating, A. Lupu, E. Marmer, R. Park, M. G. Schultz, D. T. Shindell, S. Szopa, M. G. Vivanco, O. Wild, and A. Zuber (2009), The influence of foreign vs. North American emissions on surface ozone in the US, *Atmos. Chem. Phys.*, *9*(14), 5027–5042, doi:10.5194/acp-9-5027-2009.

Russell, A. R., L. C. Valin, and R. C. Cohen (2012), Trends in OMI NO_2 observations over the US: effects of emission control technology and the economic recession, *Atmos. Chem. Phys. Discuss.*, *12*(6), 15,419–15,452, doi:10.5194/acpd-12-15419-2012.

Sandu, A., D. N. Daescu, G. R. Carmichael, and T. Chai (2005), Adjoint sensitivity analysis of regional air quality models, *J. Comput. Phys.*, *204*(1), 222 – 252, doi: 10.1016/j.jcp.2004.10.011.

Schaub, M., J. Skelly, J. Zhang, J. Ferdinand, J. Savage, R. Stevenson, D. Davis, and K. Steiner (2005), Physiological and foliar symptom response in the crowns of Prunus serotina, Fraxinus americana and Acer rubrum canopy trees to ambient ozone under forest conditions, *Environ. Pol.*, *133*(3), 553–567, doi: http://dx.doi.org/10.1016/j.envpol.2004.06.012.

Shindell, D., J. C. I. Kuylenstierna, E. Vignati, R. van Dingenen, M. Amann, Z. Klimont, S. C. Anenberg, N. Muller, G. Janssens-Maenhout, F. Raes, J. Schwartz, G. Faluvegi, L. Pozzoli, K. Kupiainen, L. Hglund-Isaksson, L. Emberson, D. Streets, V. Ramanathan, K. Hicks, N. T. K. Oanh, G. Milly, M. Williams, V. Demkine, and D. Fowler (2012), Simultaneously mitigating near-term climate change and improving human health and food security, *Science*, *335*(6065), 183–189, doi:10.1126/science.1210026.

Tong, D. Q., R. Mathur, D. Kang, S. Yu, K. L. Schere, and G. Pouliot (2009), Vegetation exposure to ozone over the continental united states: Assessment of exposure indices by the Eta-CMAQ air quality forecast model, *Atmos. Environ.*, *43*(3), 724 – 733, doi: 10.1016/j.atmosenv.2008.09.084.

U.S. EPA (2006), Air quality criteria for ozone and related photochemical oxidants (2006 Final), Washington, DC, EPA/600/R-05/004aF-cF, Available at http://cfpub.epa.gov/ncea/cfm/recordisplay.cfm?deid=149923.

U.S. EPA (2011), Regulatory Impact Analysis. Final National Ambient Air Quality Standard for Ozone (Draft), Available at http://www.epa.gov/glo/actions.html.

U.S. EPA (2013), Integrated science assessment for ozone and related photochemical oxidants (2013)), Reserach Triangle Park, NC, EPA/600/R-10/076F, Available at http://epa.gov/ncea/isa/.

van der Werf, G. R., J. T. Randerson, L. Giglio, G. J. Collatz, M. Mu, P. S. Kasibhatla, D. C. Morton, R. S. DeFries, Y. Jin, and T. T. van Leeuwen (2010), Global fire emissions and the contribution of deforestation, savanna, forest, agricultural, and peat fires (1997–2009), *Atmos. Chem. Phys. Discuss.*, *10*(6), 16,153–16,230, doi:10.5194/acpd-10-16153-2010.

Van Dingenen, R., F. J. Dentener, F. Raes, M. C. Krol, L. Emberson, and J. Cofala (2009), The global impact of ozone on agricultural crop yields under current and future air quality legislation, *Atmos. Environ.*, *43*(3), 604 – 618, doi:10.1016/j.atmosenv.2008.10.033.

Walker, T. W., D. B. A. Jones, M. Parrington, D. K. Henze, L. T. Murray, J. W. Bottenheim, K. Anlauf, J. R. Worden, K. W. Bowman, C. Shim, K. Singh, M. Kopacz, D. W. Tarasick, J. Davies, P. von der Gathen, A. M. Thompson, and C. C. Carouge (2012), Impacts of midlatitude precursor emissions and local photochemistry on ozone abundances in the Arctic, *J. Geophys. Res.*, *117*(D1), doi:10.1029/2011JD016370.

Wang, H., D. J. Jacob, P. L. Sager, D. G. Streets, R. J. Park, A. B. Gilliland, and A. van Donkelaar (2009), Surface ozone background in the United States: Canadian and Mexican pollution influences, *Atmos. Environ.*, *43*(6), 1310–1319, doi:10.1016/j.atmosenv.2008.11.036.

Wang, Y., D. J. Jacob, and J. A. Logan (1998), Global simulation of tropospheric O_3-NOx-hydrocarbon chemistry: 1. model formulation, *J. Geophys. Res.*, *103*(D9), 10,713–10,725, doi:10.1029/98JD00158.

Wiedinmyer, C., S. K. Akagi, R. J. Yokelson, L. K. Emmons, J. A. Al-Saadi, J. J. Orlando, and A. J. Soja (2011), The Fire INventory from NCAR (FINN): a high resolution global model to estimate the emissions from open burning, *Geosci. Model Dev.*, *4*(3), 625–641, doi:10.5194/gmd-4-625-2011.

Wild, O., A. M. Fiore, D. T. Shindell, R. M. Doherty, W. J. Collins, F. J. Dentener, M. G. Schultz, S. Gong, I. A. MacKenzie, G. Zeng, P. Hess, B. N. Duncan, D. J. Bergmann, S. Szopa, J. E. Jonson, T. J. Keating, and A. Zuber (2012), Modelling future changes in surface ozone: a parameterized approach, *Atmos. Chem. Phys.*, *12*(4), 2037–2054,

doi:10.5194/acp-12-2037-2012.

Wu, S., L. J. Mickley, D. J. Jacob, J. A. Logan, R. M. Yantosca, and D. Rind (2007), Why are there large differences between models in global budgets of tropospheric ozone?, */jgr*, *112*(D5), doi:10.1029/2006JD007801.

Wu, S., B. N. Duncan, D. J. Jacob, A. M. Fiore, and O. Wild (2009), Chemical nonlinearities in relating intercontinental ozone pollution to anthropogenic emissions, *Geophys. Res. Lett.*, *36*(5), doi:10.1029/2008GL036607.

Zhang, L., D. J. Jacob, M. Kopacz, D. K. Henze, K. Singh, and D. A. Jaffe (2009a), Intercontinental source attribution of ozone pollution at western U.S. sites using an adjoint method, *Geophys. Res. Lett.*, *36*(11), doi:10.1029/2009GL037950.

Zhang, L., D. J. Jacob, N. V. Downey, D. A. Wood, D. Blewitt, C. C. Carouge, A. van Donkelaar, D. B. Jones, L. T. Murray, and Y. Wang (2011), Improved estimate of the policy-relevant background ozone in the United States using the GEOS-Chem global model with 1/2 x 2/3 horizontal resolution over North America, *Atmos. Environ.*, *45*(37), 6769 – 6776, doi:10.1016/j.atmosenv.2011.07.054.

Zhang, Q., D. G. Streets, G. R. Carmichael, K. B. He, H. Huo, A. Kannari, Z. Klimont, I. S. Park, S. Reddy, J. S. Fu, D. Chen, L. Duan, Y. Lei, L. T. Wang, and Z. L. Yao (2009b), Asian emissions in 2006 for the NASA INTEX-B mission, *Atmos. Chem. Phys.*, *9*(14), 5131–5153, doi:10.5194/acp-9-5131-2009.

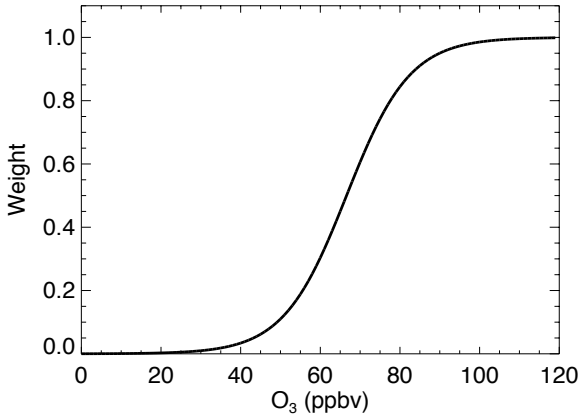

Figure 1. Weights applied to hourly ozone concentrations for W126 calculation.

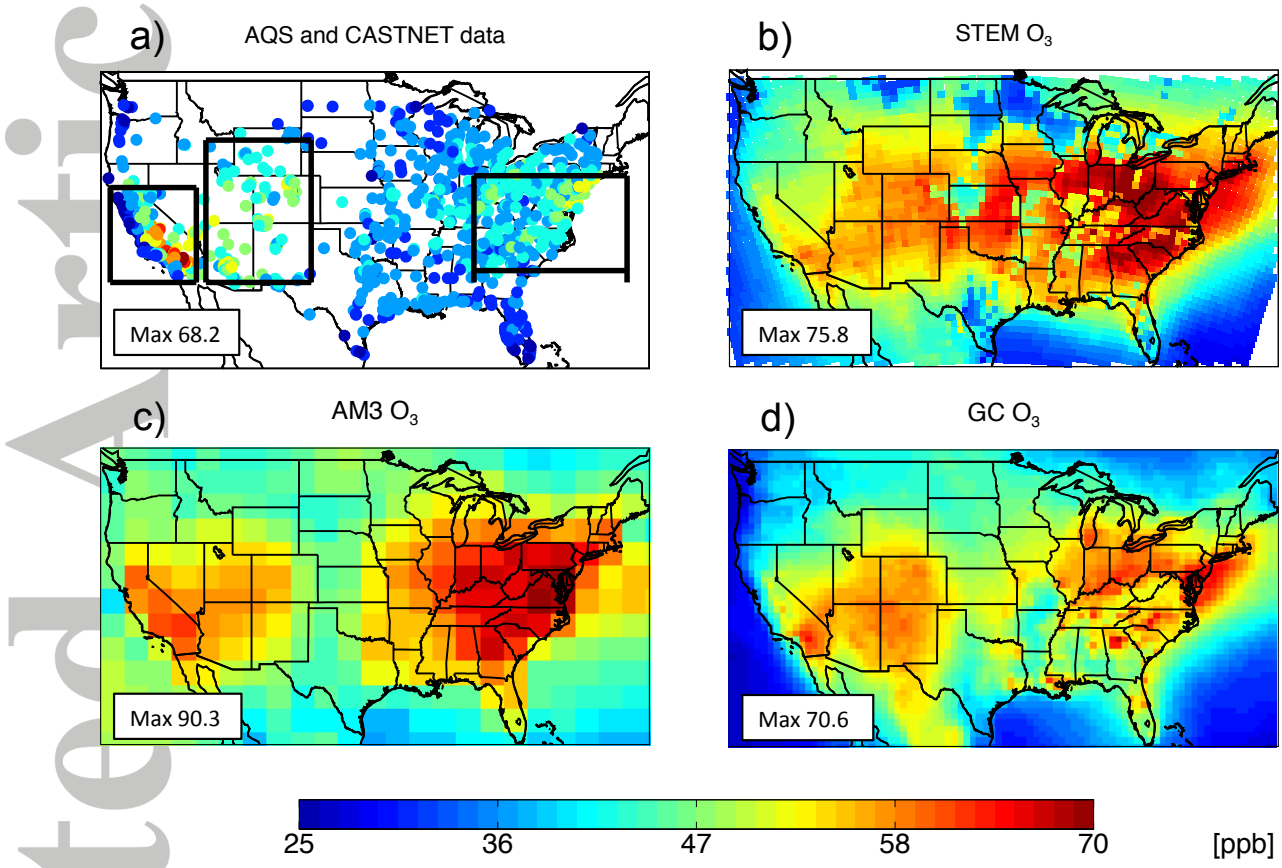

Figure 2. Three-month (May–June–July 2010) mean daytime (8 am–7 pm local time) surface ozone concentration from (a) CASTNET and AQS observations, (b) STEM, (c) AM3 and (d) GEOS-Chem. Color scales are saturated at the maximum values indicated in the legend. Black lines show the Atlantic, intermountain West and California regions discussed in text.

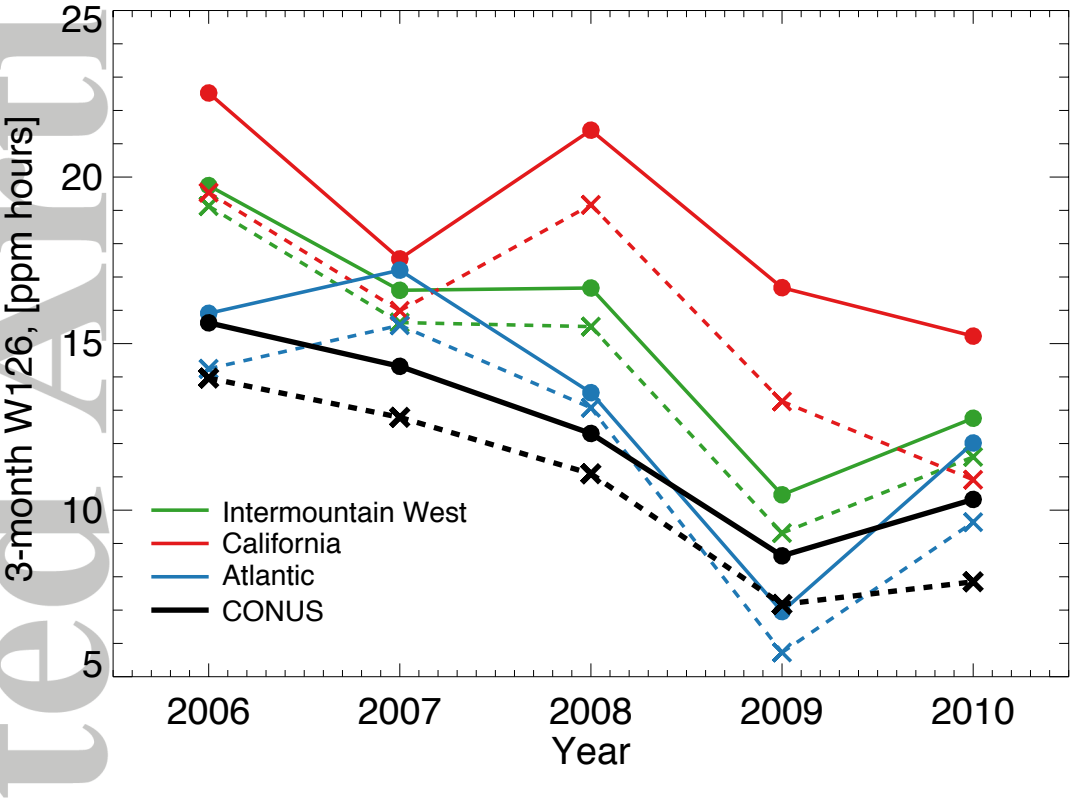

Figure 3. Time series of the spatially-averaged three-month W126 index from AQS and CASTNET in the continental U.S. and selected regions. Solid lines show the mean W126 calculated for the maximum W126 three-month sum at each station for a given year; dashed lines show the means for W126 in May–June–July.

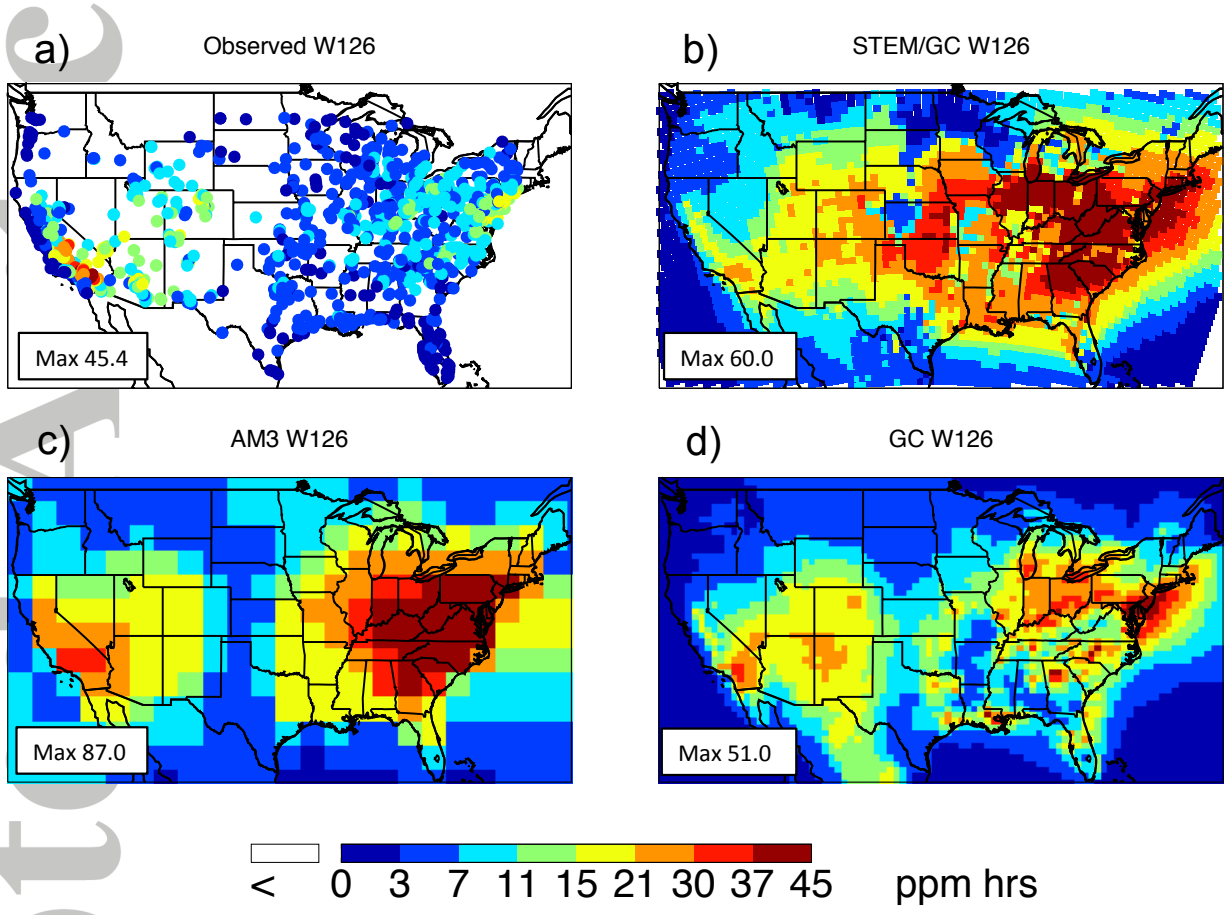

Figure 4. Three-month W126 index from (a) CASTNET and AQS observations, (b) STEM, (c) AM3 and (d) GEOS-Chem. Color scales are saturated at the maximum values indicated in the legend.

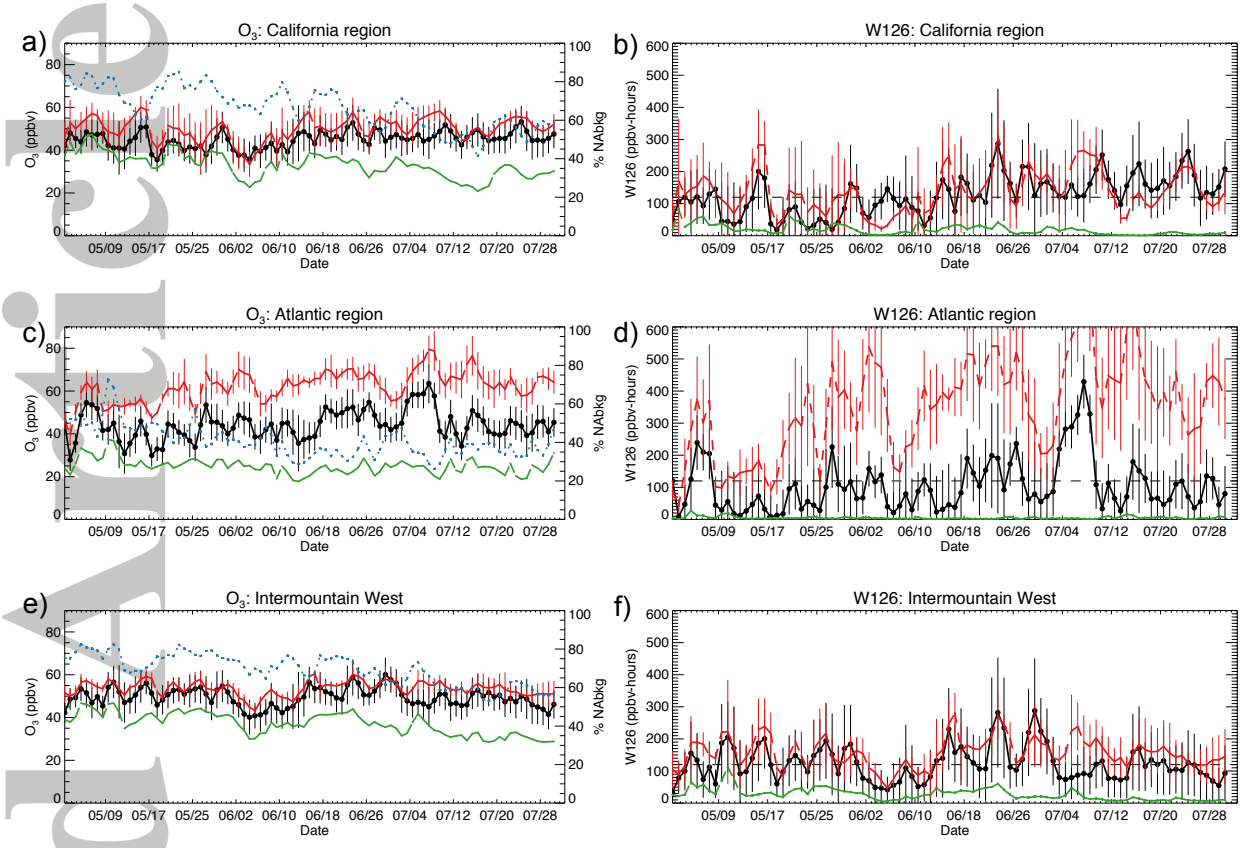

Figure 5. May–July 2010 time series of the observed and three-model mean ± standard deviation for daytime ozone (left) and daily W126 index (right) for the California (a, b), Atlantic (c, d) and intermountain West (e, f) regions. Observations from AQS and CASTNET are shown in black, model results (from three models) are shown in red. The three-model means for the North American background ozone and W126 are shown in green. The percentage contribution of the North American background to the total ozone is also shown (blue dotted line, right axis). Black dashed lines are drawn at levels above which a constant daily W126 would lead to exceedance of an 11 ppm hours standard (i.e., DI = 120 ppbv hours.) See Figure S1 in supporting information for individual model results.

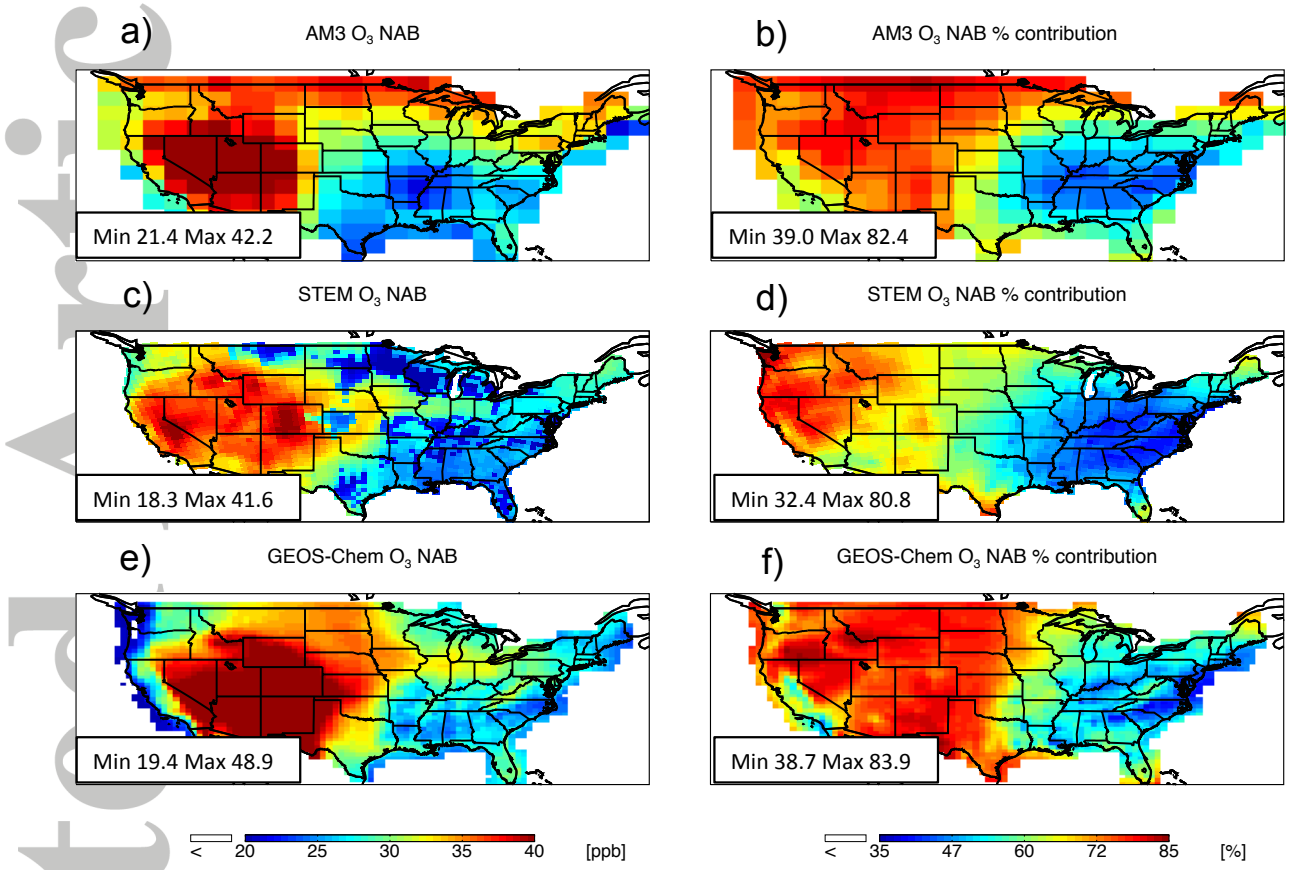

Figure 6. The 3-month North American daytime ozone background (left) and average percent contribution of NAB to daytime ozone (right) estimated with AM3 (a, b), STEM (c, d) and GEOS-Chem (e, f) models. Color scales are saturated at the minimum and maximum values indicated in the legend.

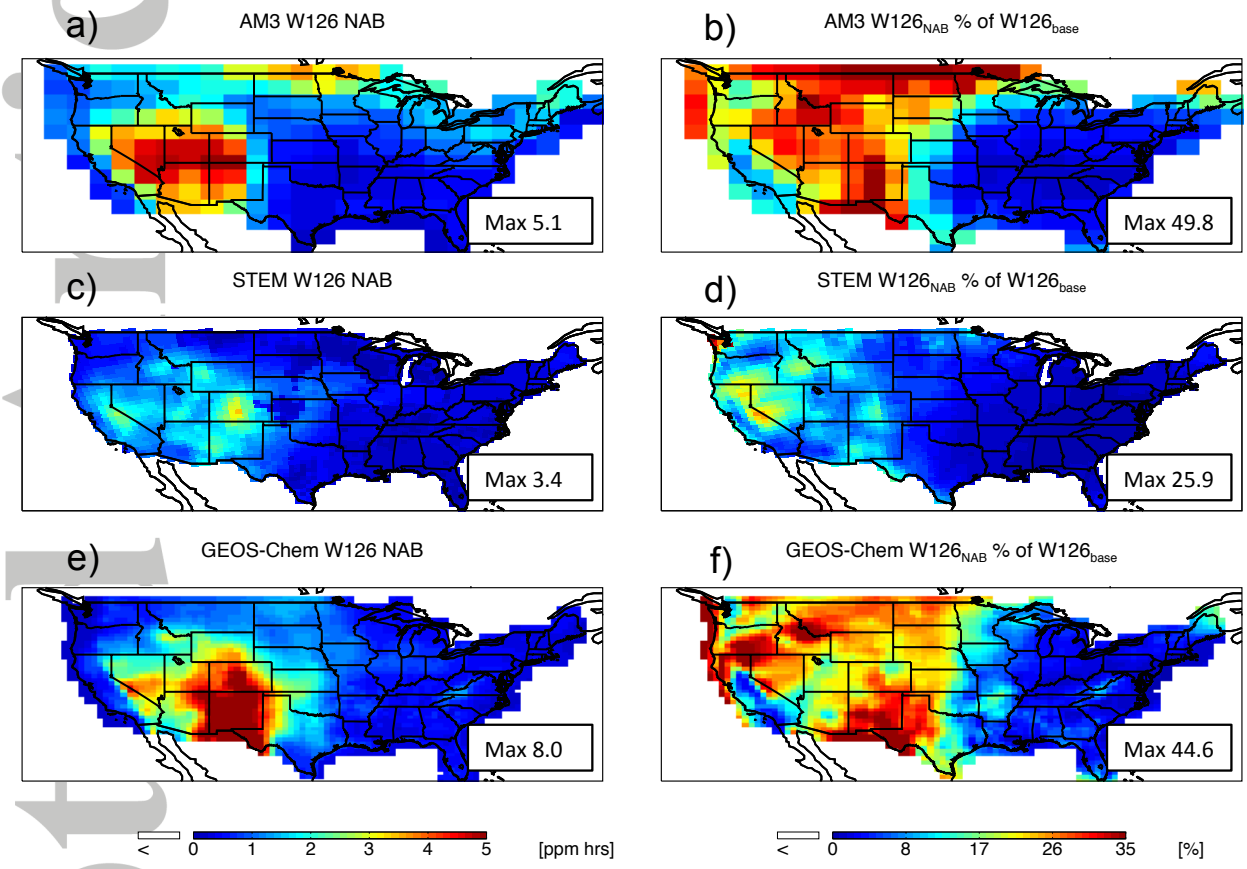

Figure 7. The 3-month North American W126 background (left) and percent NAB of total W126 (right) estimated with AM3 (a, b), STEM (c, d) and GEOS-Chem (e, f) models. Color scales are saturated at the maximum values indicated in the legend.

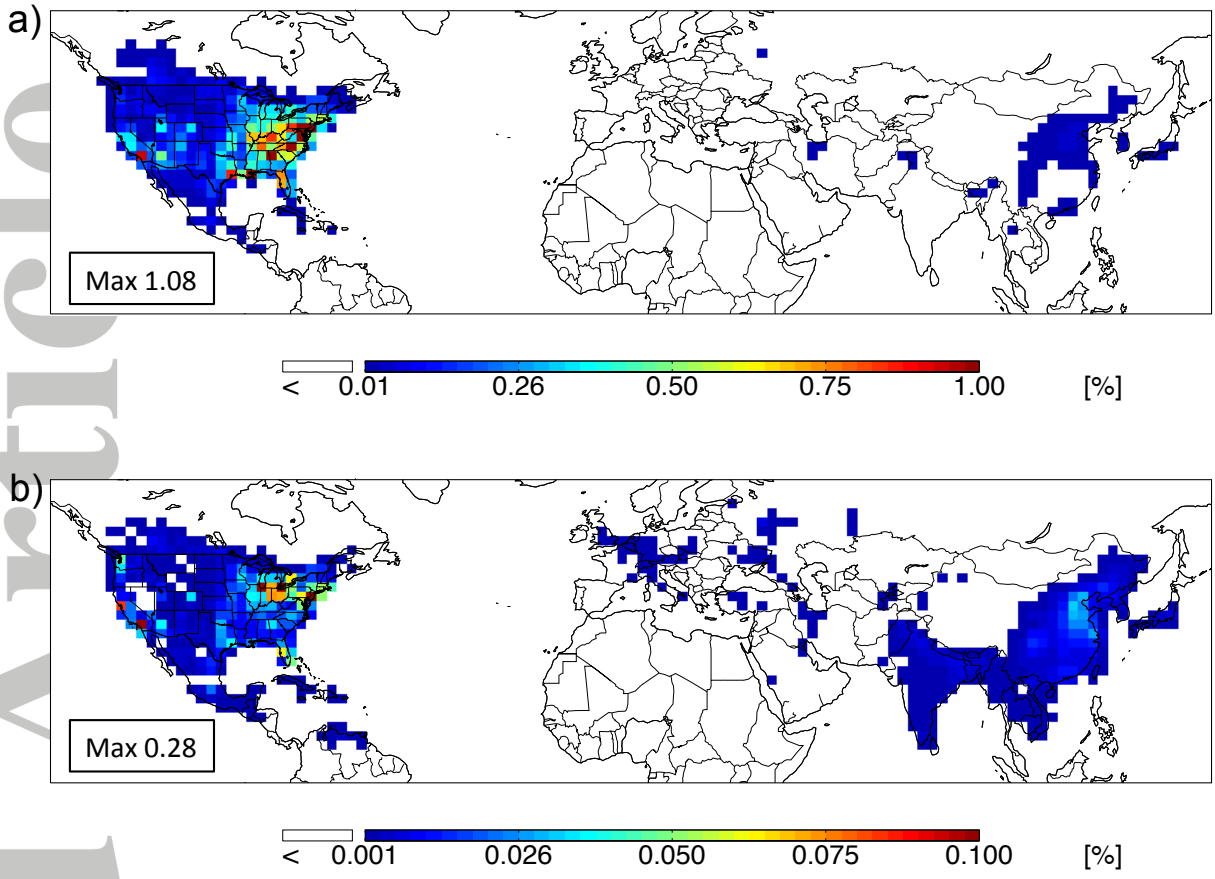

Figure 8. Sensitivities of May–July 2010 W126 in the U.S. to (a) anthropogenic NO_x and (b) anthropogenic CO emissions.

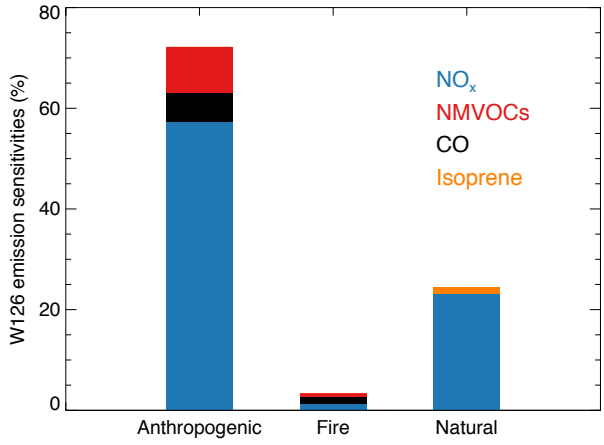

Figure 9. Sensitivities of May–July 2010 W126 in U.S. to emissions aggregated by species and sectors. Sensitivities are normalized to the total and add up to 100%.

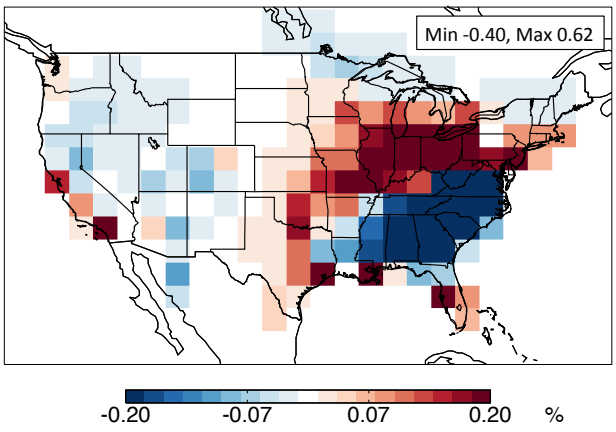

Figure 10. Sensitivities of May–July 2010 W126 in U.S. to isoprene emissions in U.S.

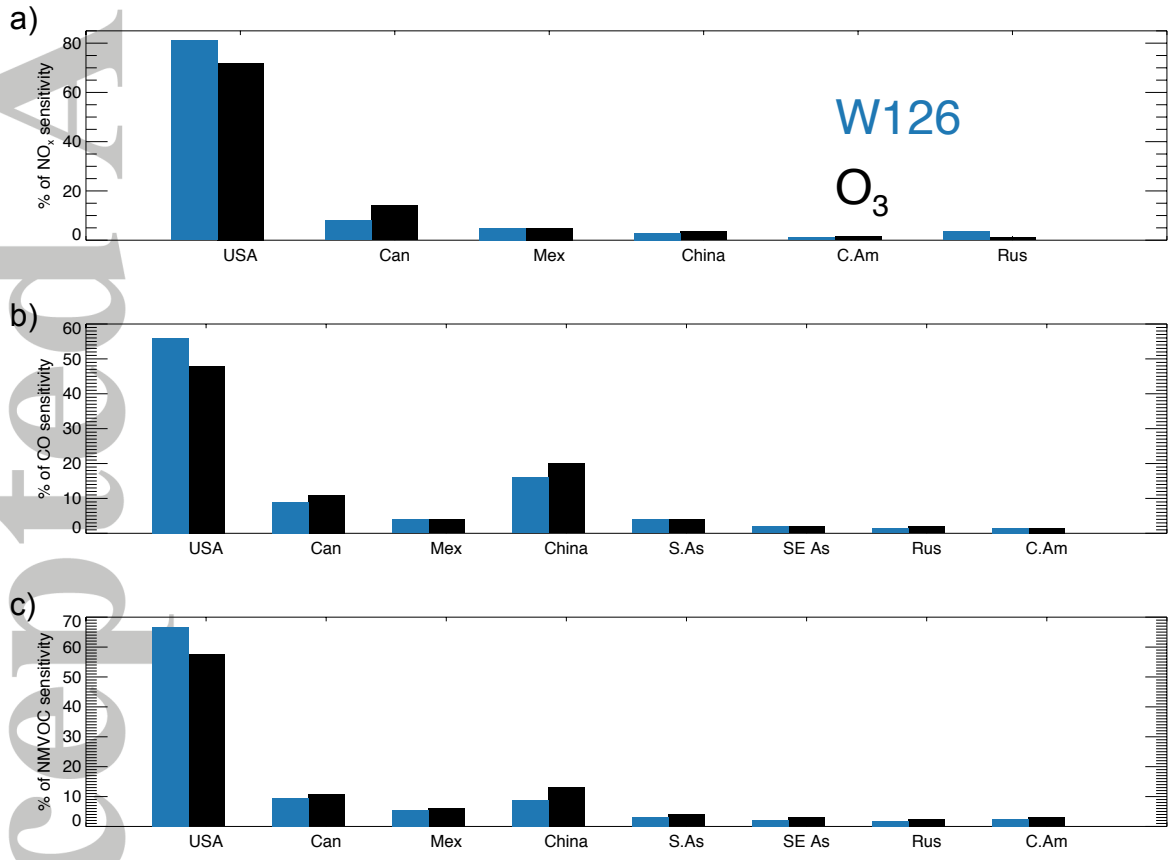

Figure 11. Sensitivities to (a) NO_x, (b) CO and (c) NMVOC emissions, aggregated by country for W126 (blue) and ozone (black). Sensitivities are normalized to the total and add up to 100% in each plot.

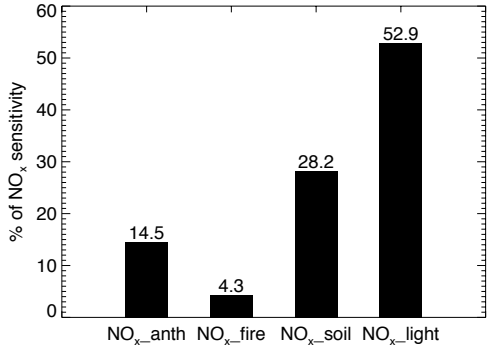

Figure 12. Sensitivities of the NAB component of W126 to NO_x emissions, aggregated by source categories. Sensitivities are normalized to the total and add up to 100%.

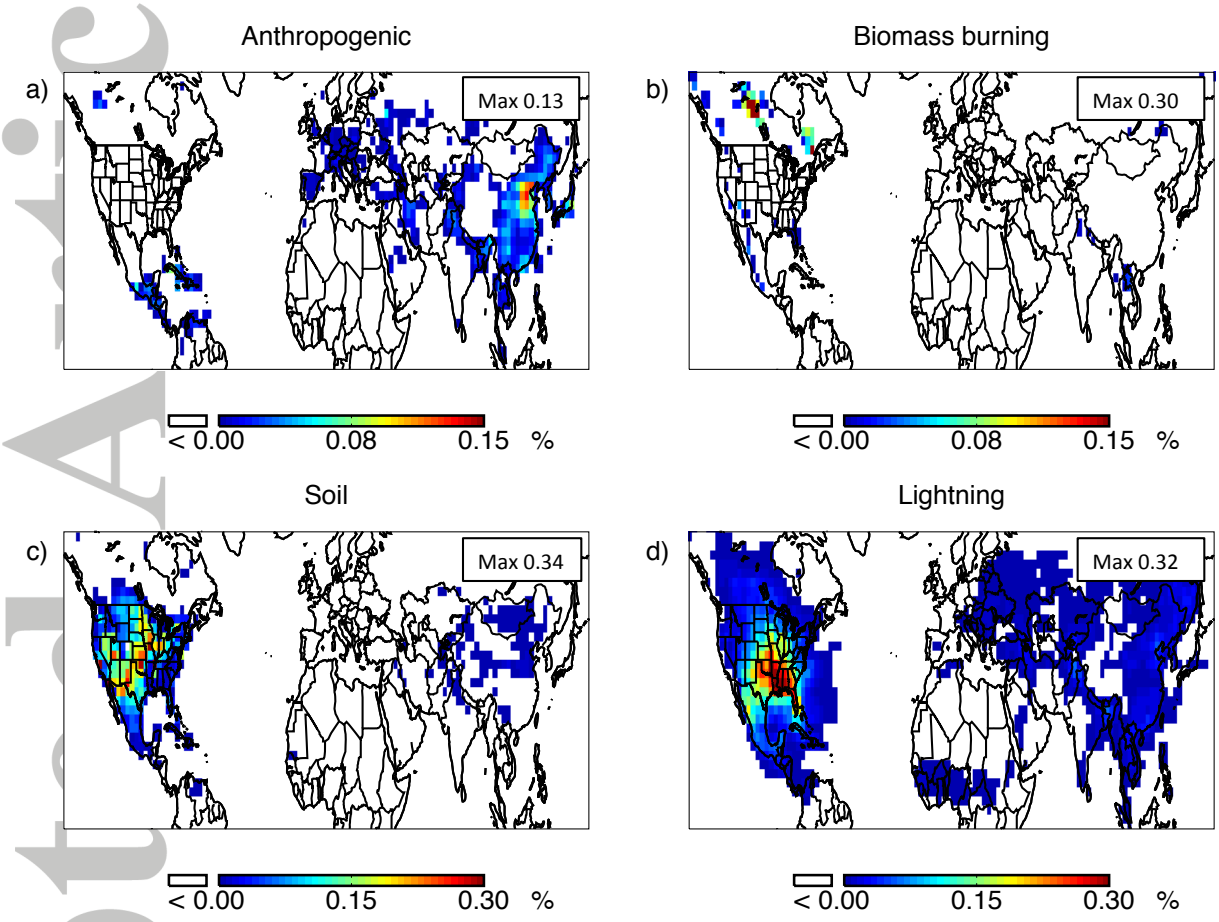

Figure 13. Normalized sensitivities of the NAB component of W126 to NO_x emissions estimates associated with (a) anthropogenic, (b) biomass burning, (c) soil and (d) lightning. Color scales are saturated at the maximum values indicated in the legend.

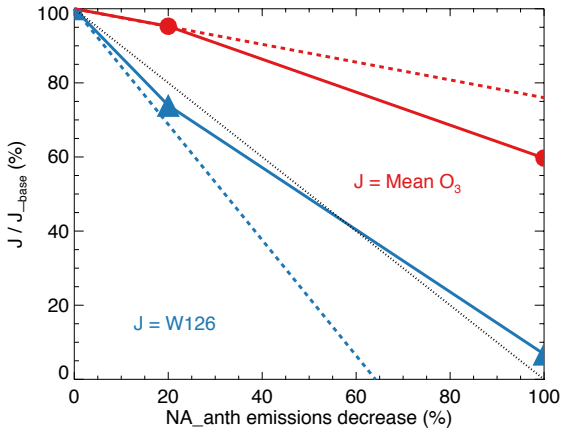

Figure 14. Change in the domain-averaged mean daytime ozone (red line with circles) and W126 (blue line with upward triangles) as a function of 20 and 100% perturbations in North American anthropogenic emissions (solid lines) in GEOS-Chem. Changes predicted from the adjoint sensitivities for the base case are shown with dashed lines. Plotted symbols indicate the relative change in cost function calculated using the perturbed emissions.

Table 1. Description of simulations/diagnostics used to determine the 3-month W126 index in the U.S. and the North American background, and to perform source attribution.

Type of simulation	Description	Model
Base	Emissions as described in the text and Table 2	GEOS-Chem, STEM, AM3
NAB	North American anthropogenic emissions set to zero	GEOS-Chem, STEM, AM3
Stratospheric tracer	Tagged stratospheric O_3S tracer originating from the stratosphere in base simulation	AM3
Adjoint	Cost function: mean 3-month W126 in the U.S., emissions as in base simulation	GEOS-Chem [a]
	Same as above, but with applied observation-based scaling factors	GEOS-Chem
	Cost function: mean 3-month daytime O_3 in the U.S., emissions as in base simulation	GEOS-Chem

[a] Adjoint GEOS-Chem runs are performed on a global scale at $2° \times 2.5°$ resolution.

Table 2. Description of the models used for W126 analysis.

Model	Horizontal resolution	Meteorology	Stratospheric O_3	U.S. anthropogenic emissions	Biogenic emissions	Biomass burning
GEOS-Chem	$1/2^\circ \times 2/3^\circ$	GEOS5 (offline)	Parameterized (Linoz)	NEI2005 scaled to 2006	MEGAN 2.0	GFED3
STEM[a]	60 km×60 km	WRF v.3.3.1	included in boundary conditions from GEOS-Chem	NEI2005	MEGAN 2.1 (based on WRF meteorology)	FINN
AM3	$2^\circ \times 2.5^\circ$	Coupled, nudged to NCEP-NCAR winds	Full stratospheric chemistry/dynamics	RCP8.5 for 2010	MEGAN 2.1	GFED3

[a] Boundary conditions for STEM are derived from global GEOS-Chem simulation at $2^\circ \times 2.5^\circ$ resolution.

Table 3. Means and coefficients of correlation for observed and modeled daytime ozone [ppbv] and W126 daily index [ppbv hours] in studied regions. [a]

Region	California				Atlantic				Intermountain West			
	O_3		W126		O_3		W126		O_3		W126	
	r	Base (NAB)	r	Base (NAB)	r	Base (NAB)	r	Base (NAB)	r	Base (NAB)	r	Base (NAB)
AM3	0.47	55.6 (36.8)	0.22	206.7 (36.9)	0.65	64.9 (29.2)	0.60	411.7 (10.2)	0.57	53.8 (39.6)	0.48	167.4 (47.0)
STEM	0.81	48.3 (33.7)	0.70	113.5 (10.4)	0.63	63.4 (19.5)	0.66	401.8 (1.4)	0.59	53.9 (32.8)	0.44	166.6 (13.0)
GC	0.75	46.0 (30.9)	0.74	110.8 (14.5)	0.70	57.9 (28.3)	0.71	249.9 (5.8)	0.57	55.5 (42.9)	0.49	177.9 (42.2)
3-model mean	0.81	50.0 (33.6)	0.66	143.7 (20.6)	0.71	62.1 (25.7)	0.71	354.5 (5.8)	0.77	54.4 (38.4)	0.69	170.6 (34.1)
Obs		44.9		125.9		44.1		102.8		49.5		122.5

[a] Shown are coefficients of correlation, r, between the model (base case) and observations, the mean values for each region for the base model run and North American background (in brackets) and for observations.